REMARKS

Dependent claim 50 has been amended to depend from claims 42-44 and 47-49, since claims 45 and 46 were cancelled. Claim 59 has been cancelled without prejudice or disclaimer. No new matter has been added. It is believed that the entry of the amendments to claim 50 and the cancellation of claim 59 would not require a new search and examination to be performed, and thus, it is respectfully requested that this amendment be entered.

Claims 33-35, 38-44, 47-50, 56-58, 61-63, 70 and 72-77 are currently pending for examination.

Rejections under 35 U.S.C. §101/§112, ¶1

Claims 33-35, 38-44, 47-50, 56-59, 61-63, 70 and 72-77 have been rejected under 35 U.S.C. §101, as the Patent Office states that the disclosed invention is inoperative for the full scope of the claims and therefore lacks utility. These claims have also been rejected under 35 U.S.C. §112, ¶1, as failing to comply with the enablement requirement, for similar reasons. The Patent Office asserts that Hirvonen, *et al.* "Effect of Diffusion Potential, Osmosis and Ion-Exchange on Transdermal Drug Deliver, Theory and Experiments," *J. Controlled Rel.* 56: 33-39 (1998) ("Hirvonen") provides evidence of the operability and unenabling of the present invention as claimed.

Initially, it should be noted that the claims as pending each recite an L-arginine or an L-arginine derivative that is applied to skin. The Applicant is not claiming that any possible substance can be delivered to the skin under the conditions specified in the claims, but rather, only the L-arginine or L-arginine derivatives as claimed. As evidence, the Applicant has provided evidence, both in the form of a declaration as well as a series of examples originally filed with the patent application, to show that L-arginine or L-arginine derivatives can be applied to the skin under such conditions.

The Patent Office has not provided any evidence that illustrates that L-arginine or L-arginine derivative cannot be successfully applied to the skin that contradicts the Applicant's evidence. Instead, the Patent Office has pointed to Hirvonen as a reference that the Patent Office asserts that one or ordinary skill in the art, in reviewing the specification, would conclude that L-

arginine and L-arginine derivatives cannot be applied to the skin of a subject as directed by the specification, despite the fact that there are working examples in the specification that teach otherwise. Hirvonen nowhere discloses or suggests the use of L-arginine or L-arginine derivative, and thus its usefulness in this regards is limited, especially in comparison with the specific evidence in the application as filed to the contrary.

In particular, Hirvonen teaches that sotalol cannot be delivered to the skin under certain conditions. The Patent Office then extrapolates, based on the sotalol data of Hirvonen, that one of ordinary skill in the art would then conclude that the invention as presently claimed is inoperable and non-enabled. However, Hirvonen is inconsistent with *itself*, thus its validity as a suitable reference would be highly questionable to one of ordinary skill in the art. In particular, Hirvonen teaches in Table 1 that for Composition VI, theoretically, there should be relatively little transport, as Hirvonen predicts $E_{dp} = 1.15$, where E_{dp} is the enhancement factor of the increase in transport relative to controls where there is no osmotic difference. However, the value actually measured (E''_{dp}) was 8.40 ± 2.74 (SE), which is not only statistically significantly greater than the theoretical value of 1.15 (by more than 2 SE units), this value was the *largest* enhancement factor actually measured by Hirvonen on Table 1. Thus, not only the validity of Hirvonen's theoretical treatment rendered suspect by its own data; Hirvonen's data also actually shows that even for sotalol, changes in osmolarity can affect molecular transport, in contrast to the position of the Patent Office.

Moreover, the formulas for sotalol and for salicylate, both discussed in Hirvonen, are not structurally similar to L-arginine or its derivatives. The formula for sotalol is shown below:

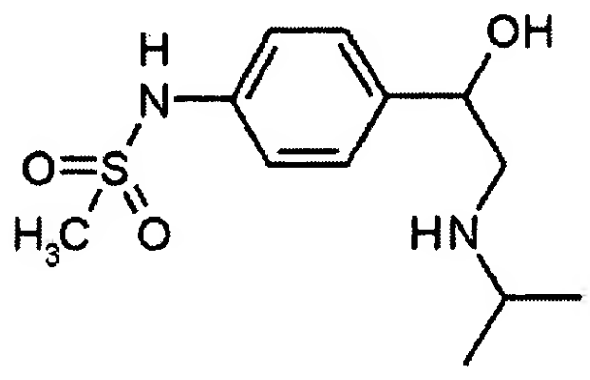

and for salicylate:

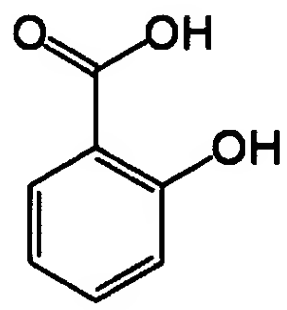

while the structure of L-arginine is as follows:

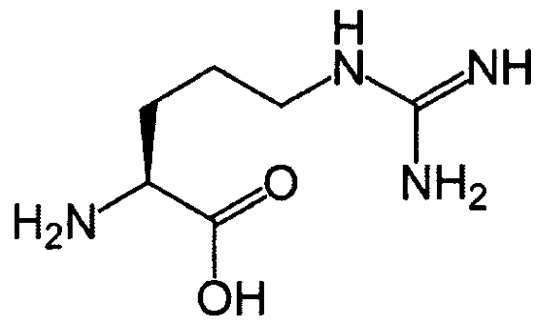

The Patent Office has not asserted that any of these chemical formulas are structurally equivalent, nor has the Patent Office has not pointed to any references that teach this, or suggest that any results obtained for sotalol or salicylate can be applied to L-arginine or L-arginine derivatives. Given the uncertainties inherent in transdermal drug delivery, as evidenced by Hirvonen (among other references in this field of study), one of ordinary skill in the art, in examining the experimental data demonstrated in Hirvonen, would not believe this data and the experimental data within the instant application to be so totally inconsistent that this person would then conclude that all of the Applicant's data does not support that L-arginine can be delivered as claimed, and all of the instant claims as pending are therefore invalid for being inoperative for their full scope.

Moreover, research into the scientific literature concerning Hirvonen reveals that Hirvonen itself is not a widely-accepted paper. In fact, to date, Applicant has been able to identify only three papers have cited Hirvonen, after a study using SciSearch. These three papers are Haldiya, *et al.*, "Dermal Ulcers and Hypertension in Salt Workers," *Current Sci.*, 87:1139 (2004) ("Haldiya") (Appendix 1); Suhonen, *et al.*," Epidermal Cell Culture Model Derived from Rat Keratinocytes with Permeability Characteristics Comparable to Human Cadaver Skin," *Eu. J. Pharm. Sci.*, 20:107 (2003) ("Suhonen") (Appendix 2); and Matuszak, *et al.*, "Thermodynamic Driving Force for Molecular Diffusion – Lattice Density Functional Theory Predictions," *J. Non-Equilib. Thermodyn.*, 31:355 (2006) ("Matuszak") (Appendix 3).

Suhonen is directed to a cell culture model, and only mentions Hirvonen in passing, and then only for the proposition that Hirvonen *successfully delivered* solatol across the skin (see Table 1, p. 109). Suhonen is concerned only with showing that solatol can likewise be delivered across cultured epidermal cells, rather than skin.

Haldiya was a study of workers exposed to high salt concentrations (brine), who exhibited ulcers or hypertension. According to the paper, salt concentrations did positively affect the incidence of ulcers and hypertension. Such effects would not be observed if the salt concentrations had no effect on the skin. In this paper, Hirvonen was cited for the proposition that "When salt concentration in fluid surrounding the skin is high, osmotic pressure and ion-exchange make a significant contribution to flux enhancement by diffusion potential" (p. 1140, second column, first paragraph), contradicting the position of the Patent Office regarding Hirvonen.

Matuszak appears to be the only paper that mentions the theoretical model of Hirvonen. However, Matuszak states that the diffusion potential gradient for diffusive flux in Hirvonen is only an approximation, and thus should not be treated as a universal linear law. See p. 359, paragraph 2. In other words, Matuszak states that Hirvonen's theoretical equations have only limited applicability. In fact, the equations that were derived in the Matuszak reference appear to support the Applicant's findings that transport can occur through the skin under such conditions. Thus, a person of ordinary skill in the art that is aware of Hirvonen would also be aware of Matuszak, which corrects Hirvonen's equations, and would accordingly not question, based on Hirvonen, whether agents for creating a hostile biophysical environment could be used to cause transport across the skin to occur.

Accordingly, given that Hirvonen has been published now for more than 10 years, the relative lack of citations by others in the scientific community indicates that Hirvonen itself is not widely accepted by those of ordinary skill in the art. Papers that reference Hirvonen only refer to the experimental data or state that Hirvonen's theoretical equations are not broadly applicable in all situations. Since Hirvonen's *own data* discredits those theoretical calculations, it should not be surprising that no other paper in the scientific literature has placed any significant weight on those calculations. Accordingly, as this evidence shows, one of ordinary

skill in the art would have no rational reason to believe any of the theoretical calculations discussed in Hirvonen in the face of contradictory experimental data (in *both* Hirvonen and in the instant application) and literature statements that do not support Hirvonen. Therefore, Hirvonen should not be relied upon to sustain this rejection under §101.

Thus, for at least these reasons, it is respectfully requested that the rejection of these claims be withdrawn.

Rejections under 35 U.S.C. §112, ¶2

Claims 50 and 59 have been rejected under §112, ¶2. Claims 50 (in part) and 59 depend from cancelled claims.

Claim 59 has been cancelled without prejudice or disclaimer. Claim 50 is a multiply-dependent claim, and the dependencies in claim 50 have been corrected. Thus, it is respectfully requested that the rejection of claims 50 and 59 be withdrawn.

Declaration

In rejecting the declaration as being insufficient to overcome the rejection of the claims, as discussed in the Office Action, the Patent Office appears to put greater weight on the theoretical treatment of Hirvonen than on the Applicant's data in both the application and in the declaration. For instance, the Patent Office states that Hirvonen teaches that different mechanism act to defeat enhancement of transdermal drug delivery at high and low electrolyte concentrations, and that Hirvonen provides a detailed theoretical discussion as to why in general enhancement of transdermal drug delivery by added electrolytes should fail and for this reason it must be assumed that in general such enhancement should fail.

However, Hirvonen teaches that this is true only for sotalol and salicylate; Hirvonen offers no data or mechanisms for L-arginine and L-arginine derivatives, and Hirvonen's theoretical model *fails* even its own experimental data for predicting transport of sotalol and salicylate, as discussed above, to say nothing of L-arginine and L-arginine derivatives. As Hirvonen's own "detailed theoretical discussion" emphasized by the Patent Office is *contradicted* by Hirvonen's own experimental data, Hirvonen's detailed theoretical discussion is

not useful for predicting the transport properties of L-arginine and L-arginine derivatives (or indeed, for even predicting the transport of sotalol or salicylate), and accordingly, Hirvonen's *failed* theoretical model cannot be used to contradict the *actual, experimental data* obtained by the Applicant.

Rejections under 35 U.S.C. §102(b)/§103(a)

Claims 33 and 61 have been rejected under 35 U.S.C. §102(b) as anticipated by, or in the alternative, under 35 U.S.C. §103(a), as being obvious over Ennen, *et al.*, Int. Pat. Apl. Pub. No. WO 95/15147 ("Ennen").

Applicant does not concede that any of the statements by the Patent Office regarding what is taught by Ennen are accurate, as the Patent Office has not provided an English translation of Ennen. However, Applicant submits herewith a translation of Ennen (Appendix 4), obtained in response to the rejections by the Patent Office in its latest Office Action. Ennen appears to be directed to the treatment of neurosensory phenomena. Ennen does not teach or suggest a hostile biophysical environment comprising an ionic salt mixture comprising choline chloride, sodium chloride, and magnesium chloride, as is recited in claim 33, nor does Ennen teach or suggest packaging selected from the group consisting of a liposome, an emulsion of collagen, and a collagen peptide. Thus, it is believed that claims 33 and 61 are not anticipated or rendered obvious by Ennen, and it is respectfully requested that the rejection of these claims be withdrawn.

CONCLUSION

In view of the foregoing remarks, this application should now be in condition for allowance. A notice to this effect is respectfully requested. If the Examiner believes, after the foregoing remarks, that the application is not in condition for allowance, the Examiner is requested to call the undersigned at the telephone number listed below.

If this response is not considered timely filed and if a request for an extension of time is otherwise absent, Applicant hereby requests any necessary extension of time. If there is a fee

Dated: May 4, 2009

Respectfully submitted,

By _____

Tani Chen, Sc.D.
Registration No.: 52,728
Patrick R.H. Waller, Ph.D.
Registration No.: 41,418
WOLF, GREENFIELD & SACKS, P.C.
Federal Reserve Plaza
600 Atlantic Avenue
Boston, Massachusetts 02210-2206
(617) 646-8000

APPENDIX 1

Dermal ulcers and hypertension in salt workers

Kripa Ram Haldiya[1,*], Murli L. Mathur[1], Raman Sachdev[1] and Habibulla N. Saiyed[2]

[1]Desert Medicine Research Centre (ICMR), Jodhpur 342 005, India
[2]National Institute of Occupational Health (ICMR), Meghani Nagar, Ahmedabad 380 816, India

In the process of salt manufacture, brine rich in salt is filled in broad pans exposed to direct sunlight. Brine workers keep their feet in the brine while working in these pans. They frequently have traumatic ulcers on their feet and hands. The aim of the present communication was to find out if prevalence of hypertension and blood pressure in brine workers was affected by the presence of ulcers on their limbs. In our cross-sectional observational study, all workers (n = 218) were clinically examined. Blood pressure was measured. Systolic and diastolic blood pressure of brine workers having ulcers on their limbs was compared with those not having the ulcers. In brine workers having ulcers, prevalence of hypertension was 15.6%, while it was 43% in those not having ulcer. Prevalence of hypertension was significantly higher in the group of brine workers with ulcers (P = 0.036) and this may be due to absorption of salt through the damaged skin.

SALT manufacturing is an important industry in Rajasthan, engaging more than 20,000 workers[1]. In the process of salt manufacture, highly concentrated brine (groundwater rich in salt, used for salt manufacture) is filled in broad pans made on the surface of land, exposed to direct sunlight. Water evaporates from this brine and sodium chloride is crystallized at the bottom of the pan. In these pans, brine workers sweep crystals of salt using broad wooden spades and make heaps of salt near the edge of the pan. Their feet and lower portion of their legs remain submerged in brine for 4 to 8 h per day. Often their upper limbs are also wet with brine or are covered with fine salt particles. They frequently sustain minor occupational injuries on their feet and hands resulting in the formation of ulcers, which heal slowly. There is a possibility of absorption of significant amount of salt through such ulcers, which in turn may affect their blood pressure. High salt content in diet is known to increase blood pressure as well as prevalence of hypertension in salt-sensitive subjects[2]. The aim of the present communication was to find out if prevalence of hypertension and blood pressure of brine workers was affected by the presence of ulcers on their limbs.

This was a cross-sectional observational study. In Rajasthan, occupational health check-up camps were held at three salt-manufacturing sites, under a project on 'Prevention and Control of Occupational Health Hazards Among the Salt Workers', sponsored by the Ministry of Health, Government of India. This project was approved by the Scientific Advisory Committee of National Institute of Occupational Health, Ahmedabad, India. The camps were organized at Sambhar, Nawa and Phalodi in collaboration with owners of salt-manufacturing units and Department of Salt, Government of India. Each camp was of five days duration. All the workers from nearby salt-manufacturing units were invited for their free health examination. The workers who were absent on the dates of the health camp were excluded from the study. All workers whose nature of job involved working in brine pans, were classified as brine workers. Brine workers who were also engaged in other processes related to salt like loading, weighing, transporting, milling or packing of salt were excluded from the analysis.

Eight hundred ninety-one salt workers attended the camps, out of which 218 who fulfilled the above inclusion criteria were taken as brine workers for the present analysis. Their age in completed years, sex, detailed occupational history, including exact nature of job and duration of working in salt industry were recorded in performa specially designed for occupational health examination.

After obtaining their informed consent, clinical examination including detailed dermatological examination was carried out by one of the authors, who did not measure blood pressure. Blood pressure of all brine workers was measured in supine position after rest of five minutes. Blood pressure was measured in the right arm using digital blood pressure equipment (Omron T-4). The cuff size was 25 cm × 13 cm. Three readings were taken by trained field investigators under the supervision of the first author. The first two readings were to familiarize the subjects with the process and the third reading was taken for analysis. The field investigators were trained to measure blood pressure for fifteen days by the authors. Body weight and height were measured by another field inves-

Table 1. Characteristics of study subjects

Characteristics	Brine workers having ulcer/s on limb/s (n = 32)	Brine workers not having any ulcer on limbs (n = 186)	P-value
Age (years)	29.72 ± 9.78	31.04 ± 8.87	0.10*
Gender M/F (%)	93.7/6.3	84.4/15.6	0.16**
Literacy (%)	37.5	33.3	0.65**
Income (Rs per annum)	23740 ± 10076	23456 ± 14615	0.10*
Smokers (%)	56.3	46.8	0.32**
Alcohol users (%)	9.4	8.1	0.80**
BMI kg/m^2	18.69 ± 2.06	18.81 ± 2.14	0.10*
Duration of salt work (years)	10.63 ± 9.17	10.91 ± 7.03	0.10*
Vegetarians (%)	65.6	64.5	0.90**

*Student's t test was applied.
**Chi-square test was applied.

*For correspondence. (e-mail: haldiyakr@rediffmail.com)

Table 2. Prevalence of hypertension (HT) according to age

	Brine workers having ulcers		Brine workers not having ulcers	
Age in years	No. examined	Prevalence of HT (%)	No. examined	Prevalence of HT (%)
15–19	4	0.0	17	0.0
20–29	13	15.4	62	4.8
30–39	5	20.0	68	2.9
40–49	9	22.2	32	3.1
50+	1	0.0	7	28.6
Total	32	15.6*	186	4.3*

*$\chi^2 = 4.39$, $P = 0.036$.

tigator trained for the purpose. Height was measured in centimetres, using anthropometric rod, while the subject stood erect on a flat platform. Body mass index (BMI) was calculated as [(weight in kg/height in metres)^2]. Systolic and diastolic blood pressure of brine workers having ulcers on their limbs was compared with those not having ulcers. Hypertension was defined as systolic blood pressure more than 139 and/or diastolic blood pressure 90 or above. Student's t test and chi-square test were used to study statistical significance of the differences.

Out of 218 brine workers, 32 (14.7%) had ulcer/s on their hands, feet or lower portion of their legs. The characteristics of the study subjects are depicted in Table 1 and were comparable in brine workers with ulcers and those without ulcers. Both groups did not have significant difference in prevalence of smoking, alcohol use, age, literacy, income, duration of working in salt industry and BMI.

Prevalence of hypertension was significantly higher in those with ulcer (15.6%) than in those not having ulcer/s (4.3%) ($\chi^2 = 4.39$, $P = 0.036$; odds ratio = 4.12). All hypertensive workers with ulcers had systolic hypertension, but diastolic blood pressure in all of them was less than 90 mm of mercury.

Mean systolic blood pressure in those having ulcers was 121.84 ± 12.42 mm of mercury and in those not having ulcers was 117.73 ± 12.13 mm of mercury. The difference was statistically not significant ($t = 1.77$, df = 216, $P = 0.08$). Mean diastolic blood pressure in those having ulcers was 67.44 ± 10.65 mm of mercury and in those not having ulcers was 69.11 ± 8.82 mm of mercury; the difference was not statistically significant ($t = 0.96$, df = 216, $P > 0.10$).

In the present study, overall prevalence of hypertension among brine workers was 6.0%, which was higher in those having ulcers (15.6%; Table 2). Higher prevalence of hypertension was consistently observed in all age groups in workers having ulcers, while among workers not having ulcers, prevalence of hypertension was high only in those above 50 years of age. However, hypertension has not been found to be an occupational health problem of rock salt-mine[3] and harbour workers[4]. Overall prevalence of hypertension in rural population of northwest India[5–8] has been found to be 3.4–7.2%.

In India, salt is mainly manufactured from the sea shore and subsoil brine. Rajasthan is the second largest producer of salt from subsoil brine in India. Salt workers are low-paid and do not use gum boots or other safety measures. As a result, their skin is often damaged by salt crystals and the spade used for sweeping them. Brine workers work in pans containing concentrated brine and their feet and lower legs remain submerged in brine. The present study depicts higher prevalence of hypertension among brine workers having ulcers on their limbs. A probable explanation of this observation may be the possibility of absorption of salt through the skin. When salt concentration in fluid surrounding the skin is high, osmotic pressure and ion-exchange make a significant contribution to flux enhancement by diffusion potential. Presence of ulcers on the skin is likely to increase salt absorption as percutaneous absorption of various substances, including salt is known to be higher through damaged skin[10–12]. This might cause elevation of blood pressure in brine workers having damaged skin, though this hypothesis needs to be confirmed. Zhou *et al.*[2] studied the relationship of dietary patterns with blood pressure in ten population groups and found mean daily intake of sodium showed significant positive association with both systolic and diastolic blood pressure in all groups, except the fishermen. This observation supports our hypothesis as percutaneous absorption of varying quantity of salt among fishermen may be the cause for lack of association between dietary salt intake and blood pressure in them. The limitation of the study is that the workers were not followed and it could not be known whether hypertension disappears after healing of ulcers or discontinuation of work for few days. Furthermore, biochemical investigation of serum and urinary electrolytes could not be done due to lack of facility. Frequent damage of skin and subsequent healing may be an important risk factor for development of hypertension in salt workers. Further studies are needed to elucidate our findings.

1. Haldiya, K. R., Mathur, M. L., Sachdeva, R., Beniwal, V. K., Singh, M. B., Yadav, S. P. and Lakshminarayana, J., Morbidity pattern of desert population engaged in salt manufacture in Rajasthan. *J. Indian Med. Assoc.*, 1995, **93**, 95–97.

2. Zhou, B. F. *et al.*, Dietary patterns in 10 groups and the relationship with blood pressure. Collaborative Study Group for Cardiovascular Diseases and Their Risk Factors. *Chin. Med. J.*, 1989, 102, 257–261.
3. O'Sullivan, J. J. and Parker, G. D., Investigation of the blood pressure levels of workers occupationally exposed to salt. *Occup. Med. (London)*, 1992, 42, 15–18.
4. Skrobonja, A. and Kontosic, I., Arterial hypertension in correlation with age and body mass index in some occupational groups in the harbour of Rijeka, Croatia. *Ind. Health*, 1998, 36, 312–317.
5. Malhotra, P., Kumari, S., Kumar, R., Jain, S. and Sharma, B. K., Prevalence and determinants of hypertension in an un-industrialized rural population of North India. *J. Hum. Hypertens.*, 1999, 13, 467–472.
6. Goel, N. K. and Kaur, P., Role of various risk factors in the epidemiology of hypertension in a rural community of Varanasi district. *Indian J. Public Health*, 1996, 40, 71–76.
7. Kumar, P. and Chaudhary, V., Epidemiological study of hypertension in a rural community of western Rajasthan. *Indian Heart J.*, 1991, 43, 43–45.
8. Jajoo, U. N., Kalantri, S. P., Gupta, O. P., Jain, A. P. and Gupta, K., The prevalence of hypertension in rural population around Sevagram. *J. Assoc. Physicians India*, 1993, 41, 422–424.
9. Hirvonen, J., Murtomaki, L. and Kontturi, K., Effect of diffusion potential, osmosis and ion-exchange on transdermal drug delivery: theory and experiments. *J. Control Release*, 1998, 56, 33–39.
10. Moon, K. C., Wester, R. C. and Maibach, H. I., Diseased skin models in the hairless guinea pig: *in vivo* percutaneous absorption. *Dermatologica*, 1990, 180, 8–12.
11. Bronaugh, R. L. and Stewart, R. F., Methods for *in vitro* percutaneous absorption studies V: Permeation through damaged skin. *J. Pharm. Sci.*, 1985, 74, 1062–1066.
12. Shani, J. *et al.*, Skin penetration of minerals in psoriatics and guinea-pigs bathing in hypertonic salt solutions. *Pharmacol. Res. Commun.*, 1985, 17, 501–512.

ACKNOWLEDGEMENTS. Ministry of Health and Family Welfare, Govt. of India had financed the project on salt workers working in desert areas of Gujarat and western Rajasthan. We thank the Salt Commissioner, Government of India and his team for cooperation.

Received 12 March 2004; revised accepted 14 June 2004

Is River Ghaggar, Saraswati? Geochemical constraints

Jayant K. Tripathi[1,*], Barbara Bock[2], V. Rajamani[1] and A. Eisenhauer[2]

[1]School of Environmental Sciences, Jawaharlal Nehru University, New Delhi 110 067, India
[2]IFM GEOMAR, Leibniz-Institut für Meereswissenschaften, Wischhofstrasse, 1-3, D-24148 Kiel, Germany

The identity of the river along which the famous Harappan Civilization developed and the causes of the demise of this culture are topics of considerable debate. Many of the Harappan sites are located along the ephemeral Ghaggar river within the Thar Desert in the northwestern India and adjacent Pakistan. The Ghaggar was also thought to be the mythical river Saraswati, which was described as glacial-fed river. Sr and Nd isotopic composition of the Ghaggar alluvium as well as Thar Desert sediments suggests a Sub-Himalayan sediment source, with no contribution from the glaciated regions. The development of extensive Harappan Civilization all along the Ghaggar suggests a catchment with high monsoon rainfall. It is likely that with the changes in the monsoon scenario after 3500 BC could have gradually dried up the Ghaggar river and resulted in the migration and/or extinction of the Harappan Civilization on this river.

THE largest and the oldest urban civilization of the world was the Indus Valley (Harappan) Civilization of northwest India and Pakistan[1]. Almost two-thirds of nearly 1500 archaeological sites of this civilization occur on the dried banks of the Ghaggar river[2] (Figure 1). The River Ghaggar originating in the Sub-Himalayas flows through the northern part of the Thar today as an ephemeral river mainly during the SW monsoon season and disappears in the desert. However, the river seems to have played a key role in the development of the Harappans[2,3]. The Ghaggar river has been identified with the mighty glacial-fed river Saraswati[4–6], which is described in the oldest religious document written in Sanskrit, the *Rig-Veda* (1500 BC)[7,8]. Based on geomorphological studies and identification of clasts in the river channels of outer Himalayas, it has been suggested that the palaeo-Ghaggar (alias Saraswati) had its catchment in the glaciated Higher Himalayas[9,10]. Another prevalent hypothesis is that the ancestral channels of Yamuna and Satluj once fed the Saraswati[9,11]. The antecedent Yamuna and Satluj rivers originate from the glaciated Higher and Tibetan Himalayas respectively, and limit the expansion of the Thar Desert in the east and north. If water availability is the key climate determinant for life[12] and the region was already experiencing aridity[13], the palaeo-Ghaggar must have been perennial for the Harappans to flourish. To identify the source (glaciated or non-glaciated terrains) and the nature (perennial or ephemeral) of the palaeo-Ghaggar and, therefore, to understand the likely cause of the social collapse of the Harappans, we have studied Sr and Nd isotopic characteristics of the sediments deposited by desert-forming processes and by the River Ghaggar in the Thar Desert region of northwestern India and compared these with the values of other Himalayan rivers in the region and with those of various Himalayan lithotectonic units.

Recycled sediments formed due to cannibalistic processes of erosion and subsequent deposition pose difficulties for the identification of their sources. However, in the Himalayan orogen, Sr and Nd isotopes have been successfully used to identify different lithostratigraphic zones[14] and to locate the source areas of sediments of the Tertiary foreland basins[15,16], Bengal fan[17] and those of the present-day Himalayan rivers[18]. Identification of sediment

*For correspondence. (e-mail: jktrip@yahoo.com)

APPENDIX 2

Available online at www.sciencedirect.com
SCIENCE DIRECT®
European Journal of Pharmaceutical Sciences 20 (2003) 107–113
EUROPEAN JOURNAL OF PHARMACEUTICAL SCIENCES
www.elsevier.com/locate/ejps

Epidermal cell culture model derived from rat keratinocytes with permeability characteristics comparable to human cadaver skin

T. Marjukka Suhonen[a,*], Sanna Pasonen-Seppänen[b], Merja Kirjavainen[a,1], Markku Tammi[b], Raija Tammi[b], Arto Urtti[a]

[a]*Department of Pharmaceutics, University of Kuopio, P.O. Box 1627, FIN-70211 Kuopio, Finland*
[b]*Department of Anatomy, University of Kuopio, Kuopio, Finland*

Received 3 April 2003; received in revised form 16 June 2003; accepted 23 June 2003

Abstract

The permeability characteristics of an organotypic epidermal culture model derived from rat epidermal keratinocytes, ROC, and isolated human cadaver epidermis, HEM, were compared. Rat epidermal keratinocyte (REK) cell line was grown for 3 weeks on collagen gel in the absence of feeder cells in culture inserts at an air–liquid interface. Transdermal permeabilities of 18 compounds ranging from 92 to 504 in molecular weight and from −4.3 to 3.9 in log of octanol–water partition coefficient, charged or uncharged, were measured in the culture model and isolated human epidermis. The REK organotypic culture model (ROC) provided a close estimate of human epidermal permeabilities over the whole range of the solutes used with on the average of 2-fold higher permeability coefficients (range 0.3–5.2) than those obtained from isolated human cadaver epidermis. The easily maintained and reproducible ROC model may be useful in screening transepidermal drug permeabilities together with possessing potential for research on dermal formulations, irritation, toxicity and gene therapy.

Keywords: Cell culture; Keratinocyte; Transdermal; Permeability; Drug delivery

1. Introduction

Adequate skin permeation is a prerequisite for successful (trans)dermal drug therapy. Isolated human or animal skin is commonly used in drug permeability assessment. The problems involved with isolated skin samples include their variable quality and lack of viability.

It is widely acknowledged that organotypic epidermal culture models may be used to replace the human cadaver and animal skin that are difficult to obtain and be standardized for routine permeability testing of drugs. Several skin cell culture models have been presented in the literature. Typically, they are either derived from primary or early passage cells, e.g. (Fartasch and Ponec, 1994; Kennedy et al., 1996; Stark et al., 1999) or from continuous cell lines (Boelsma et al., 1999; Schoop et al., 1999). These cultures are generally supported by feeder cells (Asbill et al., 2000; Boyce and Williams, 1993; Pouliot et al., 1999; Schoop et al., 1999) or de-epidermized dermis (Cumpstone et al., 1989; Fartasch and Ponec, 1994; Kennedy et al., 1996; Mak et al., 1991).

Keratinocytes maintained at the air–liquid interface have been shown to stratify, express several differentiation markers, and form an apparently normal stratum corneum (Fartasch and Ponec, 1994; Mak et al., 1991; Parenteau et al., 1991; Schoop et al., 1999; Slivka et al., 1993). However, it has been difficult to produce an organotypic culture model with a permeability barrier comparable to that of intact skin (Asbill et al., 2000; Cumpstone et al., 1989; Mak et al., 1991; Nolte et al., 1993; Ponec et al., 1990; Regnier et al., 1993; Roy et al., 1993; Schmook et al., 2001). Typically, the permeabilities of the cultured skin alternatives, derived either from human or animal skin, have been several orders of magnitude higher than that of intact human skin in vitro. In addition, so far no extensive evaluation of drug permeabilities with a large set of compounds with a variety of physicochemical characteristics in any cultured epidermal models has been done. This is obviously a serious defect in the use of cultured epidermis if they are to be used to predict human skin permeability, and may lead to erroneous conclusions.

*Corresponding author. Tel.: +358-17-163-454; fax: +358-17-162-252.
E-mail address: marjukka.suhonen@uku.fi (T. Marjukka Suhonen).
[1]Present address: Orion Corporation Orion Pharma, Kuopio, Finland.

0928-0987/03/$ – see front matter
doi:10.1016/S0928-0987(03)00176-3

The purpose of the present study was to evaluate a novel permeability model, which, at the same time, would be relatively simple and easily maintained. Recently, an organotypic epidermal culture model utilizing a continuous keratinocyte cell line derived from newborn rat skin (REK) was shown to differentiate into epidermis with normal stratum corneum ultrastructure and functional permeability barrier as measured by transepidermal water loss (TEWL) and by permeability of corticosterone (Pasonen-Seppänen et al., 2001a,b). Namely, after 3 weeks in culture, the transepidermal water loss values and the permeability coefficient for corticosterone, a lipophilic solute, were close to those measured in intact human cadaver epidermis. The present work further explores the permeability barrier properties of the REK organotypic culture (ROC) model. It is shown for the first time that the permeability coefficients of ROC for a large number of solutes with different lipophilicities, molecular weights, and charges are close to those measured in intact human cadaver skin in vitro.

2. Materials and methods

2.1. Materials

Cell culture media. Minimal essential medium (MEM, without L-glutamine) and Dulbecco's MEM (DMEM, with 4500 mg/l glucose) were obtained from Gibco-BRL (Life Technologies, Paisley, Scotland), as well as Earle's Balanced salt solution (EBSS, 10×), and 7.5% sodium bicarbonate solution. Fetal bovine serum (FBS) was obtained from HyClone (Logan, UT, USA). L-Glutamine (200 mM), penicillin–streptomycin solution (containing 10 000 U penicillin and 10 mg/ml streptomycin in 0.9% sodium chloride), trypsin–EDTA solution (containing 500 U/ml porcine trypsin and 180 μg/ml EDTA in Dulbecco's phosphate-buffered saline), and L-ascorbic acid were from Sigma (St. Louis, MO, USA). Transwell tissue culture inserts (24 mm diameter, 3.0 μm pore size) were from Costar (Cambridge, MA, USA). Aqueous acetic acid and sodium chloride were of standard laboratory grade.

For permeation studies, phosphate-buffered saline (pH 7.4, prepared from PBS tablets, Sigma) was used. The radiolabeled permeants (fructose-1-^{3}H(*N*))-sucrose (12.3 Ci/mmol), D-(1-^{3}H(*N*))-mannitol (26.3 Ci/mmol), 3-*O*-(methyl-^{3}H)-methyl-D-glucose (81.5 Ci/mmol), (2-^{3}H)-glycerol (16.0 Ci/mmol), D-(1,2,6,7-^{3}H(*N*))-aldosterone (70.0 Ci/mmol), (1,2,6,7-^{3}H(*N*))-corticosterone (70.0 Ci/mmol), (1α,2α-^{3}H(*N*))-testosterone (51.0 Ci/mmol), (6,7-^{3}H(*N*))-estradiol (44.0 Ci/mmol), and (7-^{14}C)-salicylic acid (55.5 Ci/mmol) were obtained from NEN Life Science Products (Boston, MA, USA), and ^{3}H(G)-raffinose (20.0 Ci/mmol) from American Radiolabeled Chemicals (St. Louis, MO, USA), all at higher than 97% purity according to the manufacturers and used as such. The β-blocking agents atenolol, sotalol hydrochloride, nadolol, pindolol, metoprolol tartrate, alprenolol hydrochloride, and propranolol hydrochloride were obtained from Sigma, except for timolol maleate, which was donated by Merck, Sharp & Dohme Research Laboratory (Rahway, NJ, USA), all at higher than 98% purity and used as such. The physicochemical properties of the solutes used are presented in Table 1.

2.2. Keratinocyte culture

The rat epidermal keratinocyte cell line (REK) was derived from neonatal rat epidermal keratinocytes (a generous gift from Dr. Donald K. MacCallum, Ann Arbor, MI, USA) originally isolated by Baden and Kubilus (Baden and Kubilus, 1983). Stock cultures were grown in MEM with 10% fetal bovine serum, 4 mM L-glutamine, 50 μg/ml streptomycin sulfate and 50 U/ml penicillin at 37 °C in humidified 95% air/5% CO_2. The REKs were subcultured twice a week by incubating them for approximately 5 min at 37 °C in trypsin–EDTA solution. The REK cell line was tested to exclude the possibility of *Mycoplasma* contamination.

2.3. Collagen substrate

Approximately 1 g of collagen strands from three to four rat tails was removed, washed with 70% ethanol and allowed to dry under UV light. Dry collagen strands were weighed and sterile aqueous acetic acid (0.1%, v/v) was added to give a final concentration of 3 mg/ml. The mixture was stirred for 48 h at 4 °C and then centrifuged for 2 h at 2000×*g*. The clear supernatant was stored at 4 °C. To prepare collagen supports, the collagen was mixed with EBSS, 7.5% sodium bicarbonate, and 1 M sodium hydroxide solution, at a volume ratio of 80:10:3:2, respectively, in an ice bath. To cover the entire growth surface, 1 ml of the mixture was pipetted onto individual tissue culture inserts and incubated overnight at 37 °C in a humidified atmosphere to polymerize collagen, and rinsed briefly with the culture medium before use.

2.4. REK organotypic culture (ROC)

Recently confluent cultures of REKs with no morphological evidence of stratification were trypsinized, diluted with DMEM with 10% FBS, 4 mM L-glutamine, 50 μg/ml streptomycin sulfate and 50 U/ml penicillin, and 2 ml of the cell suspension (200 000 cells/ml) was applied onto the collagen substrates on the Transwell culture inserts. The subcultivated REKs were grown for 3 days with culture medium present both in the well beneath the insert as well as on the surface of the cells. The culture was subsequently air-lifted (i.e., medium removed from the surface of the cells) and the level of the medium beneath the insert adjusted to the level of REKs present on the collagen gels (approximately 1.5 ml). The culture medium was supplemented with 40 μg/ml ascorbic acid from the day after the culture was configured at the air–liquid interface. The cultures were grown for 3 weeks, with the medium changed every 2 days for the first week and daily

Table 1
The physicochemical and permeation properties of the solutes used in the present study

Solute	log $K_{oct/w}$[a]	MW[b]	Cadaver epidermis				Refs.	Cultured epidermis			
			$P\times10^7$ (cm/s)[l]	T_{lag} (h)[m]	n[n]	$P_{Lit}\times10^7$ (cm/s)[o]		$P\times10^7$ (cm/s)[l]	T_{lag} (h)[m]	n[n]	P_{cell}/P_{skin}[p]
Raffinose	−4.30[c]	504	0.14±0.09	8–21	8	0.04	Peck et al. (1994)	0.10±0.006	20–22	3	0.7
Sucrose	−3.70[d]	342	2.04±1.46	6–25	11	0.12	Peck et al. (1998)	1.45±1.21	8–20	9	0.7
Mannitol	−3.10[e]	182	1.95±1.16	5– 20	12	0.55	Zhu et al. (2001)	6.29±1.95	9–22	21	3.2
Methylglucose	−2.50[c]	194	0.58±0.34	2–12	14			0.39±0.15	1–15	9	0.7
Salicylic acid	−2.14[h]	138	0.94±0.86	0–3	11	1.90	Sims et al. (1992)	0.24±0.10	0–1.5	13	0.3
Glycerol	−1.96[g]	92	2.74±1.26	3–7	10			8.25±0.63	5–12	6	3.0
Atenolol	−1.77[h]	266	0.30±0.10	0–22	6	0.14	Modamio et al. (2000)	1.02±0.22	0	4	3.4
Sotalol	−1.44[h]	272	0.24±0.10	0–24	7	0.26	Hirvonen et al. (1998)	0.19±0.09	25–33	5	0.8
Nadolol	−1.06[h]	309	0.22±0.09	3–25	8			0.22±0.11	25–35	5	1.0
Pindolol	−0.33[h]	248	0.55±0.23	7–20	7			0.64±0.37	26–36	7	1.2
Metoprolol	0.03[h]	267	0.83±0.33	10–21	7	2.30	Modamio et al. (2000)	0.99±0.47	10–35	7	1.2
Timolol	0.09[h]	316	0.81±0.53	0–23	8			2.22±1.03	18–30	8	2.7
Alprenolol	0.65[h]	249	4.54±1.86	1–9	8			11.1±1.30	0–2	6	2.4
Aldosterone	1.08[j]	360	0.27±0.17	2–12	7	0.16	Johnson et al. (1995)	0.31±0.05	4–10	7	1.1
Propranolol	1.37[h]	259	4.21±2.25	0–9	18	4.90	Modamio et al. (2000)	8.50±2.67	0–6	10	2.0
Corticosterone	1.94[j]	347	1.62±0.84	1–10	13	0.89	Buchwald and Bodor (2001)	2.71±1.08	1–3	19	1.7
Testosterone	3.32[k]	288	20.5±9.37	1	9	15.0	Johnson et al. (1996)	103±32.0	0.5–1	9	5.0
β-Estradiol	3.86[f]	272	23.1±6.13	0–2	11	17.0	Knutson et al. (1993)	119±43.8	0.5–1	9	5.2

[a] Log of octanol–water partition coefficient.
[b] Molecular weight.
[c] From Yoneto et al. (1995).
[d] From Johnson et al. (1997).
[e] From Hansch and Leo (1979).
[f] From Hansch et al. (1995).
[g] From de Gier (1993).
[h] Log of octanol/pH 7.4 buffer partition coefficient. Calculated according to Schoenwald and Huang (1983); Wang et al. (1991).
[j] From Johnson et al. (1996).
[k] From Yalkowsky et al. (1983).
[l] Permeability coefficient (mean±S.D.).
[m] Lag time of permeation.
[n] Number of individual samples (for cadaver skin, samples were from several donors; for culture, samples were of at least two passage numbers).
[o] Permeability data obtained from the literature as referenced in Ref. column.
[p] The permeability coefficient of cultured epidermis divided by the permeability coefficient of cadaver epidermis.

thereafter. Histology and ultrastructure of the cultures were evaluated periodically in a manner similar described in previous reports from our group (Pasonen-Seppänen et al., 2001a,b).

2.5. Permeation studies

For the permeation experiments, 3-week-old REK organotypic cultures (ROC) or human epidermal membrane (HEM) was used. Cadaver abdominal skin was obtained from the Kuopio University Hospital (Kuopio, Finland) with the permission from The National Board of Medicolegal Affairs. The excised skin was heated in distilled water at 60 °C for 2 min before the epidermis was separated form the underlying dermis, dried, and frozen for later use. Prior to mounting the pieces of skin into diffusion chambers, the frozen skin samples were allowed to thaw at room temperature, and hydrated briefly in PBS prior to mounting the skin in the diffusion cells.

The permeation studies for both HEM and ROC were carried out using two-chamber diffusion cells (Side-Bi-Side, Crown Glass Company, Somerville, NJ, USA) with a 3-ml volume in each compartment and an average effective diffusional area of 0.64 cm^2. Briefly, the membrane was clamped between the cell-halves with the stratum corneum side facing the donor chamber. HEM was hydrated overnight in PBS at 37°C prior to the experiment. Continuous magnetic stirring was maintained in both chambers. At the beginning of an experiment, the receiver chamber was replaced with fresh buffer. The donor chamber was replaced with a solution containing 1 mM of each of the β-blockers studied in PBS (pH 7.4). Alternatively, the donor was spiked with a radiolabeled test substance (20 000–40 000 dpm/10 μl). The concentrations used were far below the solubility limits of the solutes. Aliquots were withdrawn at predetermined time intervals (typically, 10 μl from the donor and 200 μl from the receiver chamber). The same volume of fresh buffer was added back to the receiver to maintain a constant volume. The samples were analyzed for the β-blocking agents by HPLC (see below). The radiolabeled samples were mixed with 3 ml of scintillation cocktail (UltimaGold, Packard, Bioscience, Groningen, The Netherlands) and analyzed by a liquid scintillation counter (WinSpectral 1414, Wallac, Finland).

Permeability experiments were run long enough to

ensure that the steady-state phase was clearly reached and maintained (typically, total time for data collection was at least three times the lag time). The permeability coefficients (P, cm s^{-1}) for the probe permeants were calculated at steady state under sink conditions according to Eq. (1):

$$P = \frac{1}{AC_D}\frac{dQ}{dt} \quad (1)$$

where A is the diffusional area of the diffusion cell (cm^2), C_D is the concentration in the donor chamber (dpm ml^{-1} or $\mu g\ ml^{-1}$), and dQ/dt (dpm $s^{-1}\ cm^{-2}$ or $\mu g\ s^{-1}\ cm^{-2}$) is the slope of the linear region of the cumulative amount of permeant in receiver chamber (Q, dpm or μg) versus time (t, s) plot with the r^2 values being in the range of 0.941–1.000, except for the slow penetrating permeants such as atenolol and sucrose where $r^2 = 0.799–1.000$.

The integrity of the skin samples, and presence of air bubbles were monitored visually throughout the study. The data from chambers showing a decrease in medium volume, a significant decrease (i.e., more than 5%) in donor concentration, or an abrupt increase in the steady-state slope, were discarded.

The experimental data obtained with ROC and HEM for the 18 compounds studied was fitted with Eq. (2):

$$\log P\ (\text{cm s}^{-1}) = \alpha \cdot \log K_{oct} + \beta \cdot \text{MW} + \gamma \quad (2)$$

where P is skin permeability (cm s^{-1}), K_{oct} is octanol–water partition coefficient, MW is molecular weight, and α, β, and γ are constants. The multiple regression analysis was performed using the SigmaPlot 4.01 software (SPSS Science, Chicago, IL, USA).

2.6. HPLC assay

A Beckman Gold HPLC system (Berkeley, CA, USA) with a Kromasil 100 C8 column (5 μm, 4.6 mm×15 cm, Higgins Analytical, Mountain View, CA, USA) was used to determine the β-blocker concentrations in the samples at 30 °C using gradient HPLC as described previously (Ranta et al., 2002). Calibration curves were constructed for each experimental run. The peak area was linearly related to concentration for samples containing 2–1400 ng of solutes injected onto the column. The correlation coefficients for the calibration curves were more than 0.98. The peak areas of the samples were converted to concentrations using the calibration curve.

3. Results and discussion

As recently reported, the 3-week-old ROCs supplemented with vitamin C in the present study were shown to duplicate most of the structural features of epidermis in vivo (Pasonen-Seppänen et al., 2001a,b). Histology and ultrastructure of the cultures in the present study were checked periodically. The structural features remained unchanged throughout the study (data not shown).

The permeability characteristics of the ROC remained fairly constant for almost 60 passages (about 30 weeks) in our laboratory, as studied by mannitol (Fig. 1a), a hydrophilic solute, and corticosterone (Fig. 1b), a lipophilic model solute. Permeability coefficients for these model solutes were checked periodically and used as a means to check the validity of the culture in the course of various experiments.

It is noted that the present experimental conditions included an overnight prehydration of the HEM prior to the study to ensure that the water content of the tissue would be comparable to that of the cultured epidermis (i.e., which is maintained in constant contact with the culture medium, and therefore, is considered to be fully hydrated). The long prehydration is not generally included in permeation experiments with skin. However, in general, the results from permeability experiments with HEM were found to be in line with the values reported in the literature (again, which mostly includes results from studies that are conducted without prehydration) (Table 1). Therefore, prehydration of the HEM is not considered to play a major role in altering skin permeability. Only the permeability

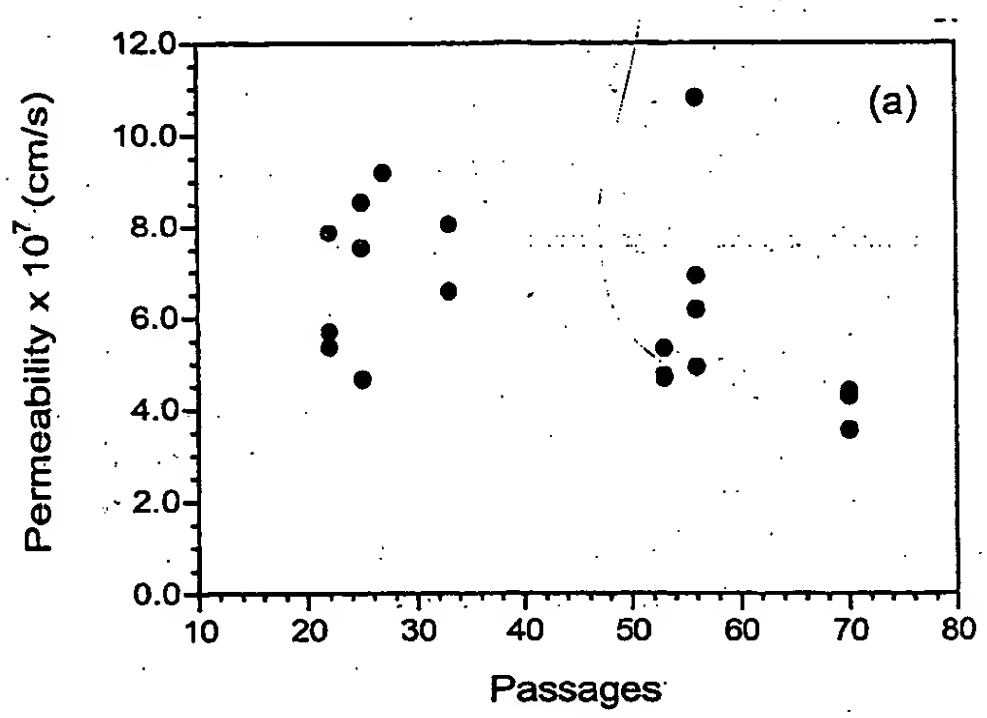

Fig. 1. Stability of the epidermal barrier properties of ROC as indicated by the permeability for (a) mannitol and (b) corticosterone in cultures raised from consecutive passages of the cell line.

coefficient for sucrose obtained in the present study was 17 times higher than that reported earlier (Peck et al., 1998), the reason for which remains unclear. A possible explanation may be found from the non-Gaussian distribution of human skin permeabilities (Williams et al., 1992).

As illustrated in Fig. 2, the permeability of ROC for the various solutes mimics closely that of HEM. There is a general increase in permeability with an increase in octanol–water partition coefficient in both model membranes. However, the ROC permeability seems to be more sensitive to changes in lipophilicity of the model solutes. With the exception of mannitol, it is shown that below log K of approximately −2.0, the permeability of ROC for the model solutes underestimates HEM permeability, whereas at above log K of 0.0, the permeability of ROC is usually somewhat higher than that of HEM (with again one outlier, aldosterone, for which the permeabilities of ROC and HEM are almost equal).

To further explore the selectivity of ROC membrane and to make a comparison to that of HEM, the experimental data obtained in the present study was fitted with Eq. (2). Eq. (2) describes skin permeability in terms of the octanol–water partition coefficient (log K_{oct}) and molecular weight (MW) (α, β, and γ being constants) and it has been successfully used to fit skin permeability data from a large variety of compounds (Moss and Cronin, 2002; Potts and Guy, 1992). The resulting quantitative structure–permeability relationships (QSPR) for the compounds studied in ROC and HEM are presented in Table 2 and in Fig. 3. A multiple regression on log K_{oct} and MW according to Eq. (2) provided a fit with $r^2=0.48$ for HEM and $r^2=0.51$ for ROC. The values of the fitted parameters for HEM were found to be somewhat different than those found with human skin in the literature (Moss and Cronin, 2002; Potts and Guy, 1992), which may also indicate that the small number of compounds does not allow for accurate modeling of the data. In addition, a large number of the compounds used in the present study are not included in the models presented previously in the literature.

In general, not a very clear difference was found between the obtained values of the fitted parameters for ROC and HEM (Table 2). The α value reflects differences between the two partitioning domains, i.e., octanol ($\alpha=1$) and skin. The values lower than unity obtained for both of the membranes suggest that the partitioning domains of ROC and HEM are more polar than octanol, which parallels the findings from earlier studies (Anderson et al., 1988). The value of α for ROC (0.25±0.07) was found to be somewhat—although not significantly—larger than that for HEM (0.17±0.05) (Table 2). Consequently, ROC may be regarded as a slightly less polar partitioning domain than HEM. In general, selectivity in solute partitioning increases with decreasing polarity of the partitioning domain (Anderson et al., 1988), and, consequently, the differences in ROC permeability are greater as the solute lipophilicity is varied, which is in line with the present experimental findings (Fig. 2). The reciprocal value of β may be approximated as a measure of the average free-volume available for diffusion (Guy and Potts, 1992). ROC ($|\beta|=0.0023\pm0.0013$) and HEM ($|\beta|=0.0028\pm0.0018$), in this context, may be regarded equal. Similarly, the absolute value of γ ($|\gamma|=5.8$) for ROC is very close to that obtained for human skin ($|\gamma|=6.2$), most likely reflecting a similar mechanism of transport through the tortuous lipid domains of human skin and ROC (Guy and Potts, 1992).

The results suggest possible structural or compositional differences in the barrier domains of the membranes. Previous work on organotypic keratinocyte cultures shows that high permeability exhibited by the cultures probably reflects abnormalities in the stratum corneum lipid profile (Ponec, 1991; Vicanova et al., 1996) as well as the intercellular organization of lamellar body contents (Boyce and Williams, 1993; Fartasch and Ponec, 1994), the main determinants of the permeability barrier (Elias and Menon, 1991). It is noted that the ROC model is devoid of appendages that may provide an additional route of penetration for polar solutes in HEM. In addition, it is of interest to explore the lipid composition and structural arrangements in the intercellular lipids of ROC stratum corneum, which remain to be elucidated in further studies.

Despite of the slight differences in selection for lipophilicity among the membranes, there is a good correlation ($r^2=0.905$) between ROC and HEM in terms of overall permeability characteristics, as is evident from Fig. 4.

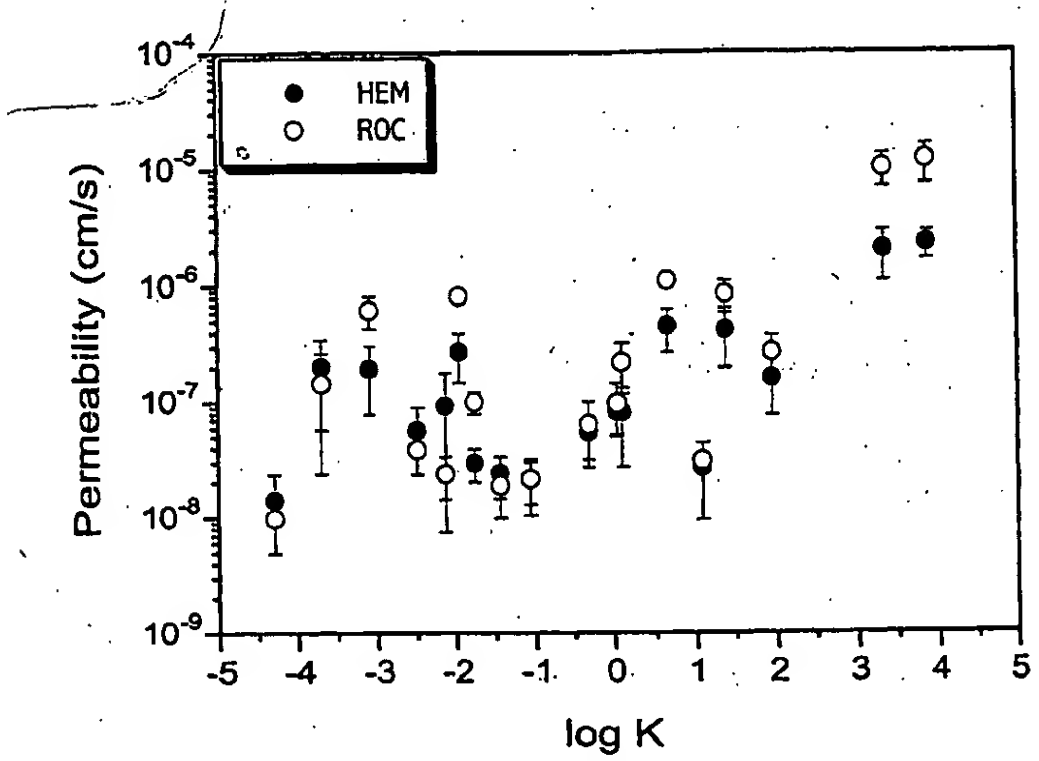

Fig. 2. The permeability coefficients (as mean±S.D.; $n=3$–21) of human cadaver epidermal membrane (HEM) and the cultured skin model (ROC) for the various solutes used in the study as a function of their octanol–water partition coefficients (log K).

Table 2
Multiple regression analysis of permeability data using Eq. (2): $\log P=\alpha \log K_{oct}+\beta\ MW+\gamma$

Membrane	α^a	$\beta^a\times10^3$	γ^a	n	r^2
HEM	0.17±0.05	−2.3±1.3	−6.20±0.38	18	0.48
ROC	0.25±0.07	−2.8±1.8	−5.84±0.51	18	0.51

[a] Value±S.D. derived from multiple regression analysis.

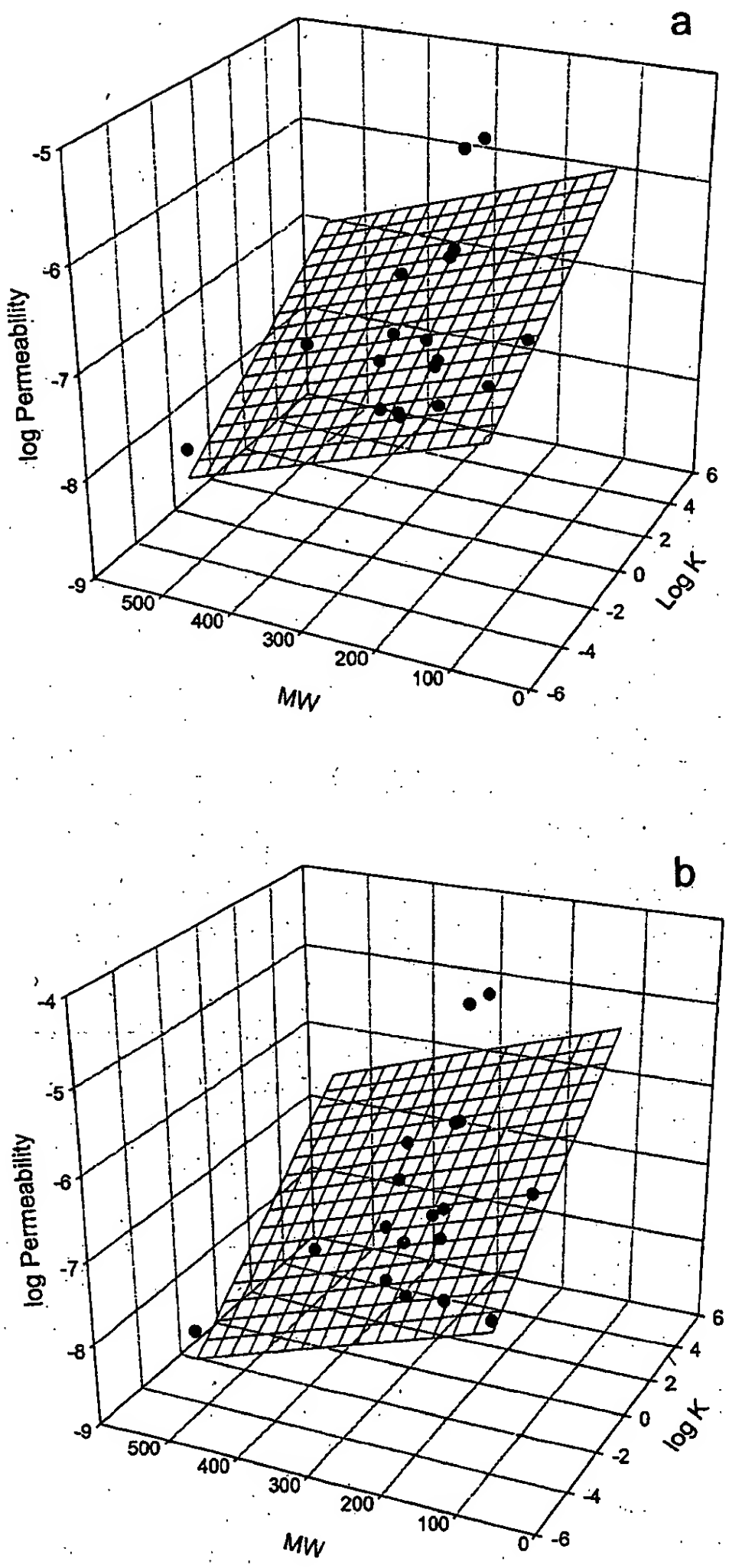

Fig. 3. A graphical representation of a multiple regression analysis of the permeability data obtained in the present study for (a) HEM and (b) ROC according to Eq. (2).

Importantly, the drug permeabilities in ROC and HEM are similar, but not identical, however. Of 18 tested compounds, 14 showed 3-fold or smaller difference in permeabilities of the model membranes. The remaining four of the 18 compounds exhibited larger than 3-fold, but less than 5.2-fold, difference in permeabilities in the two membranes. Taken together, the performance of the ROC model in predicting human skin permeabilities is reasonable.

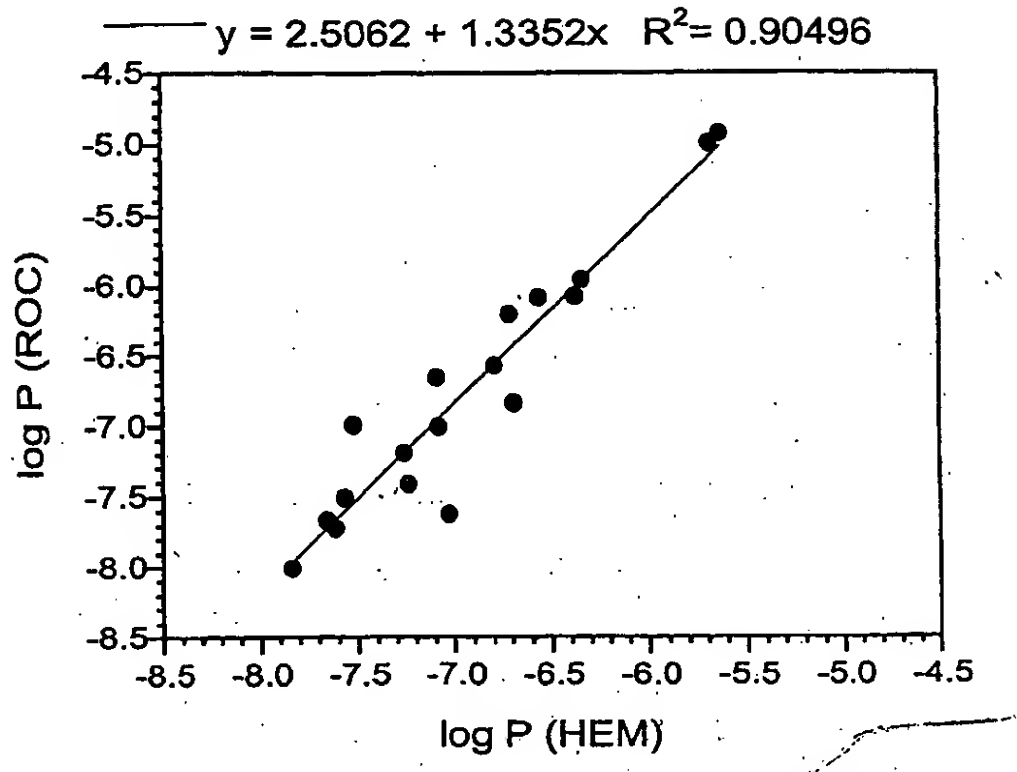

Fig. 4. The correlation between ROC and HEM permeabilities for the solutes used in the study.

The present study demonstrates for the first time that an organotypic keratinocyte culture may give a very close estimate on HEM permeabilities for solutes over a large range of lipophilicities and molecular weights. Although the present culture model is derived from rat keratinocytes it shows almost similar permeabilities and a good correlation with isolated human epidermis. A model derived from human skin cells, of course, would be more desirable, if such permeability properties could be obtained. However, at this point the ROC model seems useful for drug permeability testing. In addition, live organotypic cultures also offer potential for research on dermal formulations, irritation, toxicity and gene therapy.

Acknowledgements

The study was financially supported by the Academy of Finland, the National Agency of Technology (TEKES), and by Orion Corporation Orion Pharma. We wish to thank Ms. Milla Kainulainen and Mrs. Lea Pirskanen for skillful technical assistance, Dr. Pekka Suhonen (Orion Corporation Orion Pharma) and Erja Katainen, M.Sc. (Chem.) for their help in the regression analyses, and Veli-Pekka Ranta, M.Sc.(Pharm.) for his help in the HPLC analyses.

References

Anderson, B.D., Higuchi, W.I., Raykar, P.V., 1988. Heterogeneity effects on permeability-partition coefficient relationships in human stratum corneum. Pharm. Res. 5, 566–573.

Asbill, C., Kim, N., El-Kattan, A., Creek, K., Wertz, P., Michniak, B., 2000. Evaluation of a human bio-engineered skin equivalent for drug permeation studies. Pharm. Res. 17, 1092–1097.

Baden, H.P., Kubilus, J., 1983. The growth and differentiation of cultured newborn rat keratinocytes. J. Invest. Dermatol. 80, 124–130.

Boelsma, E., Verhoeven, M.C., Ponec, M., 1999. Reconstruction of a

human skin equivalent using a spontaneously transformed keratinocyte cell line (HaCaT). J. Invest. Dermatol. 112, 489–498.

Boyce, S.T., Williams, M.L., 1993. Lipid supplemented medium induces lamellar bodies and precursors of barrier lipids in cultured analogues of human skin. J. Invest. Dermatol. 101, 180–184.

Buchwald, P., Bodor, N., 2001. A simple, predictive, structure-based skin permeability model. J. Pharm. Pharmacol. 53, 1087–1098.

Cumpstone, M.B., Kennedy, A.H., Harmon, C.S., Potts, R.O., 1989. The water permeability of primary mouse keratinocyte cultures grown at the air-liquid interface. J. Invest. Dermatol. 92, 598–600.

de Gier, J., 1993. Osmotic behaviour and permeability properties of liposomes. Chem. Phys. Lipids 64, 187–196.

Elias, P.M., Menon, G.K., 1991. Structural and lipid biochemical correlates of the epidermal permeability barrier. Adv. Lipid Res. 24, 1–26.

Fartasch, M., Ponec, M., 1994. Improved barrier structure formation in air-exposed human keratinocyte culture systems. J. Invest. Dermatol. 102, 366–374.

Guy, R.H., Potts, R.O., 1992. Structure-permeability relationships in percutaneous penetration. J. Pharm. Sci. 81, 603–604.

Hansch, C., Leo, A., 1979. Substituent constants for correlation analysis in chemistry and biology. Wiley, New York.

Hansch, L., Leo, A., Hoekman, D., 1995. Exploring QSAR. Hydrophobic, electronic, and steric constants. Americal Chemical Society, Washington, DC.

Hirvonen, J., Murtomäki, L., Kontturi, K., 1998. Effect of diffusion potential, osmosis and ion-exchange on transdermal drug delivery: Theory and experiments. J. Control. Rel. 56, 33–39.

Johnson, M.E., Blankschtein, D., Langer, R., 1995. Permeation of steroids through human skin. J. Pharm. Sci. 84, 1144–1146.

Johnson, M.E., Blankschtein, D., Langer, R., 1997. Evaluation of solute permeation through the stratum corneum: Lateral bilayer diffusion as the primary transport mechanism. J. Pharm. Sci. 86, 1162–1172.

Johnson, M.E., Mitragotri, S., Patel, A., Blankschtein, D., Langer, R., 1996. Synergistic effects of chemical enhancers and therapeutic ultrasound on transdermal drug delivery. J. Pharm. Sci. 85, 670–679.

Kennedy, A.H., Golden, G.M., Gay, C.L., Guy, R.H., Francoeur, M.L., Mak, V.H., 1996. Stratum corneum lipids of human epidermal keratinocyte air-liquid cultures: Implications for barrier function. Pharm. Res. 13, 1162–1167.

Knutson, K., Harrison, D., Pershing, L., Goates, C., 1993. Transdermal absorption of steroids. J. Control. Rel. 24, 95–108.

Mak, V.H., Cumpstone, M.B., Kennedy, A.H., Harmon, C.S., Guy, R.H., Potts, R.O., 1991. Barrier function of human keratinocyte cultures grown at the air-liquid interface. J. Invest. Dermatol. 96, 323–327.

Modamio, P., Lastra, C.F., Marino, E.L., 2000. A comparative in vitro study of percutaneous penetration of beta-blockers in human skin. Int. J. Pharm. 194, 249–259.

Moss, G.P., Cronin, M.T., 2002. Quantitative structure-permeability relationships for percutaneous absorption: Re-analysis of steroid data. Int. J. Pharm. 238, 105–109.

Nolte, C.J., Oleson, M.A., Bilbo, P.R., Parenteau, N.L., 1993. Development of a stratum corneum and barrier function in an organotypic skin culture. Arch. Dermatol. Res. 285, 466–474.

Parenteau, N.L., Nolte, C.M., Bilbo, P., Rosenberg, M., Wilkins, L.M., Johnson, E.W., Watson, S., Mason, V.S., Bell, E., 1991. Epidermis generated in vitro: Practical considerations and applications. J. Cell. Biochem. 45, 245–251.

Pasonen-Seppänen, S., Suhonen, T.M., Kirjavainen, M., Miettinen, M., Urtti, A., Tammi, M., Tammi, R., 2001a. Formation of permeability barrier in epidermal organotypic culture for studies on drug transport. J. Invest. Dermatol. 117, 1322–1324.

Pasonen-Seppänen, S., Suhonen, T.M., Kirjavainen, M., Suihko, E., Urtti, A., Miettinen, M., Hyttinen, M., Tammi, M., Tammi, R., 2001b. Vitamin c enhances differentiation of a continuous keratinocyte cell line (REK) into epidermis with normal stratum corneum ultrastructure and functional permeability barrier. Histochem. Cell Biol. 116, 287–297.

Peck, K.D., Ghanem, A.H., Higuchi, W.I., 1994. Hindered diffusion of polar molecules through and effective pore radii estimates of intact and ethanol treated human epidermal membrane. Pharm. Res. 11, 1306–1314.

Peck, K.D., Hsu, J., Li, S.K., Ghanem, A.H., Higuchi, W.I., 1998. Flux enhancement effects of ionic surfactants upon passive and electro-osmotic transdermal transport. J. Pharm. Sci. 87, 1161–1169.

Ponec, M., 1991. Lipid metabolism in cultured keratinocytes. Adv. Lipid Res. 24, 83–118.

Ponec, M., Wauben-Penris, P.J., Burger, A., Kempenaar, J., Bodde, H.E., 1990. Nitroglycerin and sucrose permeability as quality markers for reconstructed human epidermis. Skin Pharmacol. 3, 126–135.

Potts, R.O., Guy, R.H., 1992. Predicting skin permeability. Pharm. Res. 9, 663–669.

Pouliot, R., Germain, L., Auger, F.A., Tremblay, N., Juhasz, J., 1999. Physical characterization of the stratum corneum of an in vitro human skin equivalent produced by tissue engineering and its comparison with normal human skin by ATR-FTIR spectroscopy and thermal analysis (DSC). Biochim. Biophys. Acta 1439, 341–352.

Ranta, V.-P., Toropainen, E., Talvitie, A., Auriola, S., Urtti, A., 2002. Simultaneous determination of eight b-blockers by gradient high-performance liquid chromatography with combined ultraviolet and fluorescence detection in corneal permeability studies in vitro. J. Chromatogr. B 772, 81–87.

Regnier, M., Caron, D., Reichert, U., Schaefer, H., 1993. Barrier function of human skin and human reconstructed epidermis. J. Pharm. Sci. 82, 404–407.

Roy, S.D., Fujiki, J., Fleitman, J.S., 1993. Permeabilities of alkyl p-aminobenzoates through living skin equivalent and cadaver skin. J. Pharm. Sci. 82, 1266–1268.

Schmook, F.P., Meingassner, J.G., Billich, A., 2001. Comparison of human skin or epidermis models with human and animal skin in in-vitro percutaneous absorption. Int. J. Pharm. 215, 51–56.

Schoenwald, R.D., Huang, H.S., 1983. Corneal penetration behavior of beta-blocking agents I: Physicochemical factors. J. Pharm. Sci. 72, 1266–1272.

Schoop, V.M., Mirancea, N., Fusenig, N.E., 1999. Epidermal organization and differentiation of HaCaT keratinocytes in organotypic coculture with human dermal fibroblasts. J. Invest. Dermatol. 112, 343–353.

Sims, S.M., Higuchi, W.I., Srinivasan, V., 1992. Skin alteration and convective solvent flow effects during iontophoresis. II. Monovalent anion and cation transport across human skin. Pharm. Res. 9, 1402–1409.

Slivka, S.R., Landeen, L.K., Zeigler, F., Zimber, M.P., Bartel, R.L., 1993. Characterization, barrier function, and drug metabolism of an in vitro skin model. J. Invest. Dermatol. 100, 40–46.

Stark, H.J., Baur, M., Breitkreutz, D., Mirancea, N., Fusenig, N.E., 1999. Organotypic keratinocyte cocultures in defined medium with regular epidermal morphogenesis and differentiation. J. Invest. Dermatol. 112, 681–691.

Vicanova, J., Mommaas, A.M., Mulder, A.A., Koerten, H.K., Ponec, M., 1996. Impaired desquamation in the in vitro reconstructed human epidermis. Cell Tissue Res. 286, 115–122.

Wang, W., Sasaki, H., Chien, D.S., Lee, V.H., 1991. Lipophilicity influence on conjunctival drug penetration in the pigmented rabbit: A comparison with corneal penetration. Curr. Eye Res. 10, 571–579.

Williams, A., Cornwell, P., Barry, B., 1992. On the non-gaussian distribution of human skin permeabilities. Int. J. Pharm. 86, 69–77.

Yalkowsky, S.H., Valvani, S.C., Roseman, T.J., 1983. Solubility and partitioning VI: Octanol solubility and octanol-water partition coefficients. J. Pharm. Sci. 72, 866–870.

Yoneto, K., Ghanem, A.H., Higuchi, W.I., Peck, K.D., Li, S.K., 1995. Mechanistic studies of the 1-alkyl-2-pyrrolidones as skin permeation enhancers. J. Pharm. Sci. 84, 312–317.

Zhu, H., Peck, K.D., Li, S.K., Ghanem, A.H., Higuchi, W.I., 2001. Quantification of pore induction in human epidermal membrane during iontophoresis: The importance of background electrolyte selection. J. Pharm. Sci. 90, 932–942.

APPENDIX 3

J. Non-Equilib. Thermodyn.
2006 · Vol. 31 · pp. 355–384

Thermodynamic Driving Force for Molecular Diffusion – Lattice Density Functional Theory Predictions

Daniel Matuszak, Gregory L. Aranovich, and Marc D. Donohue*
Department of Chemical and Biomolecular Engineering, The Johns Hopkins University, Baltimore, MD 21218, USA

*Corresponding author (mdd@jhu.edu)

Abstract

Fick's first law describes diffusive flux as a linear function of the concentration gradient; its most popular generalization describes flux as a linear function of the chemical potential gradient. This generalization and others have been used for modeling, but the relationships between the flux and the gradients are nonlinear because the coefficients generally depend on state variables. In this paper, lattice density functional theory equations for diffusive flux are recast into linear differential form to explore well-known diffusion equations. This shows that the diffusive flux is related to the gradients of state variables (e.g., to the chemical potential gradient) through integrating factors, much like the heat flux in Clausius's theorem is related to the difference in entropy. Subsequent analyses show why diffusive flux is more linear with respect to the fugacity gradient than the chemical potential gradient; and that the gradient of another property has linear proportionality to the diffusive flux. This property can appear as the impingement rate onto vacancies and molecules of species whose density gradients can be influenced by diffusion; and it behaves similarly to the chemical potential and the fugacity. The results agree with the theory of non-equilibrium thermodynamics about the conjugate force vectors for the diffusive flux.

1. Introduction

The description of diffusive flux in the form of a linear law is used commonly to model diffusion. The classic example is Fick's first law,

J. Non-Equilib. Thermodyn. · 2006 · Vol. 31 · No. 4
 DOI 10.1515/JNETDY.2006.015

$$\hat{J}_n = -D_n \nabla C_n, \tag{1}$$

where n indicates the species, $\hat{J}_n$ is the diffusive flux in units of molecules per area per time, D_n is the transport diffusivity; and C_n is the concentration [1–3]. Although Eq. (1) has a linear form, the proportionality between the diffusive flux and the concentration gradient is linear only when the diffusivity is constant; under these conditions, the concentration gradient appears to be the "driving force" for the process. The diffusivity can be constant for uniform systems, such as isothermal and isoviscous phases with a uniform total density; it can be predicted by using the Einstein or Stokes–Einstein relation [2, 4, 5] and by using molecular simulations [6–10]. For diffusion of vapors, the partial pressure gradient often is used to describe the diffusive flux [11],

$$\hat{J}_n = -\mathcal{P}_n \nabla P_n, \tag{2}$$

where $\mathcal{P}_n$ is the permeability, and P_n is the partial pressure of species n. For isothermal systems in the ideal-gas limit, the permeability can be written as D_n^g/kT, where the superscript "g" indicates the gas phase and kT is the thermal energy; and through membranes, the permeability can be written as the product of solubility and diffusivity. Equation (2) has a linear form, but the proportionality between the diffusive flux and the partial-pressure gradient is linear only when the permeability is constant – in such a case, the partial-pressure gradient appears to be the driving force for the process. For diffusion in nonideal solutions, the fugacity gradient can be used to model diffusion,

$$\hat{J}_n = -L_n^f \nabla f_n, \tag{3}$$

where L_n^f is the coefficient associating the diffusive flux and the fugacity gradient ∇f_n, and where the fugacity is related to the chemical potential by $\mu_n - \mu_n^{IG} = kT \ln(f_n/P_n)$. For isothermal ideal solutions, L_n^f can be written $D_n^l C_{tot}/P_n^{sat}$, where the superscript "l" indicates the liquid phase, C_{tot} is the total concentration, and P_n^{sat} is the saturation vapor pressure of species n. Equation (3) has a linear form, but the proportionality between the diffusive flux and the fugacity gradient is linear only when the coefficient L_n^f is constant – in such a case, the fugacity gradient appears to be the driving force for the process. Recent isothermal studies of multicomponent pervaporation indicate that the fugacity is the fundamental variable for describing fluxes and separation factors for zeolite membranes [12].

The fundamental driving force for diffusion often is assumed to be the chemical potential gradient. In the absence of irreversible processes that are coupled to diffusion, the diffusive flux can be written as a linear function of the chemical potential gradient,

$$\hat{J}_n = -L_n^{\mu} \nabla \mu_n, \tag{4}$$

where μ_n is the chemical potential of species n, and L_n^{μ} is the mobility [13]. Assuming that the chemical potential gradient (i) drives diffusion in general and (ii) appears as the concentration gradient for ideal systems, while expressing the chemical potential as $\mu_n = \mu_{n,o} + kT \ln(\gamma_n C_n)$ in Eq. (4), gives the Darken–Dehlinger relation [14, 15] for the transport diffusivity in Eq. (1),

$$D_n = D_n^{\circ}\left(1 + \frac{\partial \ln \gamma_n}{\partial \ln C_n}\right), \tag{5}$$

where D_n° is the self-diffusivity and γ_n is the activity coefficient. Accordingly, solutions with constant activity coefficients have a mobility L_n^{μ} that equals $D_n^{\circ} C_n / kT$, which depends on the position along a concentration gradient for a constant diffusive flux. The transport diffusivity in Eq. (5) also was derived by Onsager and Fuoss [16], and it can be written [17] as

$$D_n = D_n^{\circ} \frac{\partial \ln f_n}{\partial \ln \rho_n}, \tag{6}$$

where ρ_n is the number density. For a historical description of Eq. (6), see Reyes et al. [18]. That the chemical potential gradient drives diffusion is a paradigm that generally is attributed to Einstein [2, 4]; however, historical evidence suggests that this principle dates back to Maxwell [19]. Nevertheless, any description of the diffusive flux that assumes Eq. (4) departs from Fick's first law according to Eqs. (5) and (6), where D_n° is sometimes approximated as being constant [17]; this includes a Maxwell–Stefan formulation using $D_n^{\circ} = Đ_n$, [20].

The strongest theoretical support for Eq. (4) and, consequently, for Eqs. (5) and (6), appears in the dissipation-phenomenological equation (DPE) approach [21] of linear non-equilibrium thermodynamics (NET) [22], which restricts itself to linear phenomenological laws but admits that "It is very well possible that some irreversible processes must be described by non-linear phenomenological laws" [23]. The NET-DPE approach is "thermodynamically sound", and it can be used to analyze irreversible processes that are coupled [24]. NET describes the entropy production due to diffusive transport as a summation of net fluxes multiplied by conjugate forces, i.e., $\sum_i \hat{J}_i X_i$; and it describes the net fluxes as linear functions of these conjugate forces, i.e., $\hat{J}_i = \sum_k L_{ik} X_k$, unlike Eqs. (1)–(4), where the coupling of processes is not obvious. The conjugate forces that multiply the fluxes are sometimes called "thermodynamic forces" or "affinities", but this paper refers to them only as "conjugate forces". It is known that the phenomenological coefficients L_{ik}

generally depend on the state variables, which usually depend on position and time; this leads to nonlinearity as well as unequal partitioning of entropy production for equipartitioned forces [25, 26]. To identify the conjugate forces for the diffusive flux equation, one must describe the total entropy production of which a portion is caused by diffusive transport; for a multicomponent system we have,

$$\sigma = -\frac{\mathbf{Q}\cdot\nabla T}{T^2} - \frac{1}{T}\sum_{k=1}^{n}\hat{\mathbf{J}}_{\mathbf{k}}\cdot\left[T\nabla\left(\frac{\mu_k^\circ}{T}\right) - \mathbf{F}_{\mathbf{k}}\right] + \cdots, \tag{7}$$

where σ is the rate of entropy production per volume, $\mathbf{Q}$ is the heat flux vector, T is the temperature, the conjugate force vectors $\mathbf{X_k}$ for diffusive flux appear in brackets, the superscript in μ_k° indicates that this chemical potential neglects external fields or long-range interactions, and $\mathbf{F_k}$ is a force vector that can include contributions from an external field or long-range interactions, and the ellipsis ("...") represents entropy productions due to viscous forces and chemical reactions. For conservative forces, $\mathbf{F_k} = -\nabla\varphi_k$ where φ_k is a potential energy. By modifying the heat flux to $\mathbf{Q}' = \mathbf{Q} - \sum_k \mu_k^\circ \hat{\mathbf{J}}_{\mathbf{k}}$ in the total entropy production expression, as shown by de Groot and Mazur [23], the entropy production due to diffusive flow reduces to

$$\sigma = -\frac{\mathbf{Q}'\cdot\nabla T}{T^2} - \frac{1}{T}\sum_{k=1}^{n}\hat{\mathbf{J}}_{\mathbf{k}}\cdot\nabla\mu_k + \cdots, \tag{8}$$

where $\mu_k = \mu_k^\circ + \varphi_k$ (de Groot and Mazur write μ_k as $\tilde{\mu}_k$); in the transition between Eqs. (7) and (8), the entropy flux effectively has been transformed from $\mathbf{Q}/T$ to $\mathbf{Q}'/T$. As mentioned already, this NET–DPE result provides strong support for Eq. (4), because the conjugate-force vector in Eq. (8) is the chemical potential gradient. At the same time, the NET–DPE approach using Eq. (7) shows the limitation of Eq. (4) and, consequently, of Eqs. (5) and (6). Only recently, it has been shown in this journal [27] that Onsager's reciprocal relations are not always obeyed when the chemical potential gradient is the conjugate-force vector.

Equations (1)–(4) are examples of linear diffusion equations. Equation (4) often is considered to be a general law because the chemical potential is a fundamental thermodynamic concept, species usually migrate down their chemical potential gradients, chemical potential profiles usually are continuous at a steady state, and the equation is consistent with linear NET theory. Equation (3) has the same attributes as Eq. (4) because, historically, the fugacity has been defined directly from the chemical potential. On the other hand, Eqs. (1) and (2) are considered less general and can be less predictive

because their coefficients can be positive or negative, as well as discontinuous; e.g., the diffusivity in Eq. (1) has negative values in the case of species migrating to form separate phases that are purer than the original mixture [28]; and the permeability in Eq. (2) passes through a maximum and can be discontinuous when changing the pressure in porous materials [29–32]. Depending on the application, one of these equations may be more suitable than the others, but Eqs. (1)–(3) are considered to be forms of Eq. (4). Interestingly, the coefficient L_n^f in Eq. (3) is constant more often than L_n^μ in Eq. (4). For example, consider isothermal ideal solutions with constant diffusivities exhibiting Fickian behavior, as well as a binary isothermal system of nonideal spherical molecules undergoing equal counterdiffusion in an external field [33].

Linear diffusion equations such as Eqs. (1)–(4) are important because they are relatively intuitive and they can minimize computational overhead, e.g., when applied to multicomponent systems [34]. However, linear equations for the diffusive flux have been considered to be approximations to the Maxwell–Stefan equations [34], and they usually are written in terms of gradients that do not give a universal linear law (i.e., the following gradients are associated with coefficients that generally are not constant): the concentration gradient, the pressure gradient, the fugacity gradient, the pH gradient [35, 36], the electrostatic or diffusion potential gradient [37, 38], and the chemical potential gradient. This list can include a multitude of additional references because the problem of formulating a general linear law is more than 50 years old; therefore, interested readers are referred to the introduction in an excellent paper by Merk [39] that mentions relevant work from the early and mid-1900s.

It would be convenient to have a linear diffusion equation in terms of one gradient with a constant coefficient,

$$\hat{J}_n = \frac{J_n}{A} = -\frac{\lambda}{A}\nabla\Gamma_n, \tag{9}$$

where J_n is the diffusive flow in units of molecules per time, A is a constant cross-sectional area through which diffusive flow occurs, λ unconditionally is constant at a value of unity multiplied by the spatial unit used in evaluating the gradient, and Γ_n is the system's property that drives the diffusive flux of species n. Additionally, it would be interesting to understand the fundamental nature of the function Γ_n (e.g., is it a function of state? Why or why not?). Lastly, it would be reassuring if Eq. (9) also gave (a) the correct formulation of the Maxwell–Stefan equations, (b) correct equilibrium limits, (c) Fickian behaviour with correct departures for nonideal systems, (d) reasonable non-equilibrium phase behavior, (e) quantitative agreement with molecular

dynamics simulations, (f) a vanishing diffusive flux at the critical point, and (g) agreement with the NET–DPE approach.

We have developed a lattice density functional theory (LDFT) approach for modeling diffusion [29] as an extension of equilibrium LDFT [40–48]. The LDFT approach gives item (a), as shown in reference [49] with a detailed example for a quaternary system. Reference [29] shows that the LDFT approach gives items (b) through (d). To reinforce item (d), it can be shown [50] that the approach is consistent with the Giacomin–Lebowitz–Marra theory [51] of non-equilibrium phase transitions. Lastly, the LDFT approach can give item (e) at least for interdiffusing Weeks–Chandler–Anderson fluids in an external field [52]. In this paper, we use the LDFT approach to provide Eq. (9), to show that Eq. (9) is related to the well-known Eqs. (1)–(4) through integrating factors, and to demonstrate items (f) and (g).

2. LDFT equations for multicomponent systems

The LDFT equations for mass transfer in multicomponent systems [52] can be summarized in the following molecular balance at the general lattice site r:

$$\left.\frac{\partial \rho_n}{\partial t}\right|_r = \sum_s^{\varkappa} (j_n^{sr} - j_n^{rs}), \tag{10}$$

where the number density is limited to $0 < \rho_n(r) < 1$, $\varkappa$ is the coordination number. One-directional molecular flows (in units of molecules per time) occur between sites r and s in the lattice reference frame

$$j_n^{rs} = \frac{1}{\varkappa \tau_n(r)} \rho_n(r) \left[1 - \sum_m \rho_m(s)\right] e^{\hat{E}_n^{rs}}. \tag{11}$$

The characteristic time τ_n is related to the mean lifetime of n-type molecules at site r; the vacancy probability is $(1 - \sum_m \rho_m)$; the functional $\hat{E}_n^{rs}$ defines the influence of the reduced potential energy field on the migration of species n from site r to site s,

$$\hat{E}_n^{rs} = \begin{cases} 0; & \hat{E}_n(r) > \hat{E}_n(s) \\ -|\hat{E}_n(r) - \hat{E}_n(s)|; & \hat{E}_n(r) \le \hat{E}_n(s) \end{cases}, \tag{12}$$

where

$$\hat{E}_n(i) = \frac{\varepsilon_n(i) + \varphi_n(i)}{kT(i)}; \quad i = r, s. \tag{13}$$

The term $\varphi_n(r)$ is a particular long-range interaction or an external potential energy applied to molecules at site r; and the intermolecular interaction energy $\varepsilon_n(r)$ is a sum of nearest-neighbor contributions. For a system with only first nearest-neighbor interactions, the interaction energy can be written

$$\varepsilon_n(r) = \sum_n \varepsilon_{nm} \sum_s^{\varkappa} \rho_m(s), \tag{14}$$

where ε_{nm} is the interaction energy between nearest-neighbors of species n and m. Equation (12) is analogous to the Metropolis Monte-Carlo algorithm, in which one molecule at site r is moved to a vacant site s with a probability equal to $e^{\hat{E}_n^{rs}}$. However, this work is not based on Monte-Carlo dynamics: molecular motion occurs throughout the system; and the terms ρ_n, $e^{\hat{E}_n^{rs}}$, and τ_n in Eq. (11) are averaged quantities – readers interested in describing ρ_n with ensemble averages can do so for equilibrium as in the literature [53], but in this paper the variables are considered to be time averages.

2.1. Differential form of the diffusive flow

The diffusive flow J_n^{rs} is the difference between the forward and backward (one-directional) diffusive flows, e.g., ${}^{\downarrow}J_n^{rs} = ({}^{\downarrow}j_n^{rs} - {}^{\uparrow}j_n^{sr}) = -{}^{\uparrow}J_n^{sr}$, where the arrows indicate migration up or down a potential energy gradient. Using Eq. (11), the diffusive flow occurring down a potential energy gradient is

$${}^{\downarrow}J_n^{rs} = \left\{ \begin{array}{l} \dfrac{1}{\varkappa\tau_n(r)}\rho_n(r)\left[1 - \displaystyle\sum_m \rho_m(s)\right] \\ -\dfrac{1}{\varkappa\tau_n(s)}\rho_n(s)\left[1 - \displaystyle\sum_m \rho_m(r)\right] Exp\left(\dfrac{\varepsilon_n(s) + \varphi_n(s)}{kT(s)} - \dfrac{\varepsilon_n(r) + \varphi_n(r)}{kT(r)}\right) \end{array} \right\}. \tag{15}$$

Equation (15) can be written in differential form by using a truncated Taylor expansion to rewrite the variables at site s as variables at site r,

$$\alpha_n(s) \approx \alpha_n(r) + \lambda \left.\frac{\partial \alpha_n}{\partial x}\right|_{y,z}, \tag{16}$$

where the general character α_n can be any variable; x, y, and z are the dimensions; m includes n; whereas the distance λ separates the centers of sites r and s:

$$J_n^x(r) \approx -\lambda \frac{\rho_n(r)}{z\tau_n(r)} \left[1 - \sum_m \rho_m(r)\right] \times \left\{ \begin{array}{l} \dfrac{1}{\rho_n(r)} \dfrac{\partial \rho_n}{\partial x}\bigg|_{y,z} + \displaystyle\sum_m \left\{ \frac{z\varepsilon_{nm}}{kT(r)} + \frac{1}{1 - \sum_m \rho_m(r)} \right\} \frac{\partial \rho_m}{\partial x}\bigg|_{y,z} \\ -\dfrac{1}{T(r)} \left[\dfrac{\varphi_n(r)}{kT(r)} + \displaystyle\sum_m \frac{z\varepsilon_{nm}}{kT(r)} \rho_m(r) \right] \dfrac{\partial T}{\partial x}\bigg|_{y,z} \\ +\dfrac{1}{kT(r)} \dfrac{\partial \varphi_n}{\partial x}\bigg|_{y,z} - \dfrac{1}{\tau_n(r)} \dfrac{\partial \tau_n}{\partial x}\bigg|_{y,z} \end{array} \right\}. \quad (17)$$

In obtaining this result, nonlinear terms in λ were neglected, e.g., the product $\lambda^2[(\partial\alpha_1/\partial x)_{y,z}(\partial\alpha_2/\partial x)_{y,z}]$; this implies that $\lambda(\partial\alpha_n/\partial x)_{y,z}$ is small but non-negligible when compared to $\alpha_n(r)$. It should be repeated that the distance λ unconditionally is constant at a value of unity multiplied by the spatial units used in evaluating the derivative; the mean free path should not be equated with λ because the definition of the spatial derivative in Eq. (16) would be invalid for a varying total density. In this work, we have chosen λ to be the distance between the centers of sites r and s. The change of nomenclature also should be noted: J_n^{rs} becomes $J_n^x(r)$ when writing Eq. (15) in differential form – the net flow $J_n^x(r)$ occurs from site r in the x direction, and should not be confused with the total flow into a site at position x. Applying Eq. (16) to $^{\uparrow}J_n^{rs}$ and removing the nonlinear terms in λ also gives Eq. (17) – the logic of the piecewise Eq. (12) exists in the gradients, which can be positive or negative. Hence, the remainder of this paper only discusses the diffusive flow $J_n^x(r)$ and the diffusive flux $\hat{J}_n^x(r)$, i.e., the diffusive flow per area.

2.2. Existence of Γ_n and the path dependence of diffusive flux

Since the relationship between the diffusive flux and the gradient in Eq. (9) is linear, the objective of this work is to understand the property Γ_n and its gradient. This section constructs the property Γ_n from the LDFT approach using Eqs. (10)–(14), which have been successful at describing diffusion and phase behavior as outlined after Eq. (9). Subsequent sections characterize Γ_n and show that it produces the well-known diffusion Eqs. (1)–(4), a vanishing diffusive flux at the critical point, and agreement with the NET–DPE approach.

The diffusive flux of species n in the x direction, $\hat{J}_n^x$, is one of the components of Eq. (9),

$$\hat{J}_n^x = -\frac{\lambda}{A} \frac{\partial \Gamma_n}{\partial x}\bigg|_{y,z}, \quad (18)$$

where $A = \lambda^2$ for a cubic lattice. Combining Eqs. (17) and (18) through $\hat{J}_n^x = J_n^x/A$ gives

$$\left.\frac{\partial \Gamma_n}{\partial x}\right|_{y,z} = \frac{\partial \Gamma_n}{\partial T}\frac{\partial T}{\partial x}\bigg|_{y,z} + \frac{\partial \Gamma_n}{\partial \varphi_n}\frac{\partial \varphi_n}{\partial x}\bigg|_{y,z} + \frac{\partial \Gamma_n}{\partial \tau_n}\frac{\partial \tau_n}{\partial x}\bigg|_{y,z} + \sum_m \frac{\partial \Gamma_n}{\partial \rho_m}\frac{\partial \rho_m}{\partial x}\bigg|_{y,z}, \tag{19}$$

where

$$\begin{aligned}
\frac{\partial \Gamma_n}{\partial T} &= -\frac{\rho_n}{\varkappa \tau_n T}\left(1 - \sum_m \rho_m\right)\left[\frac{\varphi_n}{kT} + \sum_m \frac{\varkappa \varepsilon_{nm}\rho_m}{kT}\right];\\
\frac{\partial \Gamma_n}{\partial \rho_l} &= \frac{\rho_n}{\varkappa \tau_n}\left(1 - \sum_m \rho_m\right)\left[\frac{1}{1 - \sum_m \rho_m} + \frac{\varkappa \varepsilon_{nl}}{kT}\right]\\
\frac{\partial \Gamma_n}{\partial \rho_n} &= \frac{\rho_n}{\varkappa \tau_n}\left(1 - \sum_m \rho_m\right)\left[\frac{1}{\rho_n} + \frac{1}{1 - \sum_m \rho_m} + \frac{\varkappa \varepsilon_{nn}}{kT}\right];\\
\frac{\partial \Gamma_n}{\partial \varphi_n} &= \frac{\rho_n}{\varkappa \tau_n kT}\left(1 - \sum_m \rho_m\right);\\
\frac{\partial \Gamma_n}{\partial \tau_n} &= -\frac{\rho_n}{\varkappa \tau_n^2}\left(1 - \sum_m \rho_m\right).
\end{aligned} \tag{20}$$

In Eq. (19) and the subsequent equations, partial derivatives indicate the variables being held constant unless there is no indication, in which case all variables are held constant except the two variables in the differentiation. In Eq. (20), the subscript "l" represents any species in the set m except for species n.

Equation (19) is a component of the differential of Γ_n,

$$\mathrm{d}\Gamma_n = \left.\frac{\partial \Gamma_n}{\partial x}\right|_{y,z} dx + \left.\frac{\partial \Gamma_n}{\partial y}\right|_{x,z} dy + \left.\frac{\partial \Gamma_n}{\partial z}\right|_{x,y} dz, \tag{21}$$

which is written as $\mathrm{d}\Gamma_n$ because it has a nonexact differential form, i.e., second partial derivatives of Γ_n are not interchangeable:

$$\begin{aligned}
\frac{\partial}{\partial \varphi_n}\frac{\partial \Gamma_n}{\partial \tau_n} &\neq \frac{\partial}{\partial \tau_n}\frac{\partial \Gamma_n}{\partial \varphi_n} \qquad \frac{\partial}{\partial \rho_n}\frac{\partial \Gamma_n}{\partial T} \neq \frac{\partial}{\partial T}\frac{\partial \Gamma_n}{\partial \rho_n}\\
\frac{\partial}{\partial \tau_n}\frac{\partial \Gamma_n}{\partial T} &\neq \frac{\partial}{\partial T}\frac{\partial \Gamma_n}{\partial \tau_n} \qquad \frac{\partial}{\partial \rho_l}\frac{\partial \Gamma_n}{\partial \rho_n} \neq \frac{\partial}{\partial \rho_n}\frac{\partial \Gamma_n}{\partial \rho_l}
\end{aligned} \tag{22}$$

This nonexact differential form of Eq. (21) is an important mathematical consequence of a physical mechanism: diffusion between two points depends on the path between these points. Thus, $\int \bar{d}\Gamma_n$ is a path integral, which can be evaluated along a particular path or avoided by using an integrating factor.

2.3. Integrating factors in non-equilibrium processes

The classical thermodynamic example of using integrating factors is in Clausius's theorem, which gives the relation $dS = \bar{d}Q_{rev}/T$ for reversible adiabatic processes [54]. In this example, dS is the differential change in the system's entropy, $\bar{d}Q_{rev}$ is the differential amount of heat added reversibly to the system, and T is the system's temperature that is approximately equal to the heat source's temperature. The integrating factor, $1/T$, modifies $\bar{d}Q_{rev}$, creating the exact differential dS that can be integrated using only the limits of integration. This calculus shows that the heat-transfer process depends on the difference in a state variable as well as on the path between the limits that define this difference; in particular, the process depends on the path's values of T (for an irreversible process, it would be the temperature at which heat is supplied). Although integration of the resultant exact differential can be advantageous, an equivalent benefit is the identification of a continuous function with continuous partial derivatives that is very relevant to the process under investigation.

In this respect, diffusion is analogous to the heat-transfer process and, therefore, the calculus has similar features. The nonexact form of $\bar{d}\Gamma_n$ implies that the diffusive flux depends on the path between two limits – integration of $\bar{d}\Gamma_n$ is impossible unless additional information or integrating factors exist. This section shows (i) how diffusion is path-dependent, and (ii) that the driving force for the diffusive flux is related to the chemical potential gradient through an integrating factor.

Within the framework of LDFT, an integrating factor exists for $\bar{d}\Gamma_n$, yielding a well-behaved function, Υ_n, that has an exact differential,

$$d\Upsilon_n = \frac{\bar{d}\Gamma_n}{\frac{\rho_n}{\varkappa\tau_n}\left(1 - \sum_m \rho_m\right)}, \tag{23}$$

where the index m includes n. This differential $d\Upsilon_n$ is

$$d\Upsilon_n = d\ln\left(\frac{f_n b}{\varkappa\tau_n kT}\right), \tag{24}$$

where the fugacity [52] is

$$f_n = \frac{kT}{b}\frac{\rho_n}{1-\sum_m \rho_m} exp\left(\frac{\varphi_n + \varepsilon_n}{kT}\right), \tag{25}$$

and where $b = \lambda^3$ for monomers on a cubic lattice with lattice spacing λ. Equation (24) is obtained by combining Eqs. (21) and (23) then by integrating and using the definition of the fugacity – the partial derivatives in Eq. (21) are Eq. (19) and the y- and z-analogs of Eq. (19).

Combining Eqs. (9) and (23) gives

$$\hat{J}_n = -\frac{\lambda}{A}\nabla\Gamma_n = -\frac{\lambda^2}{x\tau_n} C_n \left(1 - \sum_m \rho_m\right)\nabla\Upsilon_n, \tag{26}$$

where the concentration $C_n = \rho_n/\lambda^3$. Since $f_n = P_n \exp\left(\frac{\mu_n - \mu_n^{IG}}{kT}\right)$, it follows that $\nabla\Upsilon_n = \frac{1}{kT}\nabla\mu_n$ for an isothermal and isobaric system in which $\tau_n = \tau_n(T)$; thus, the chemical potential gradient appears to drive diffusion. However, $\nabla\Upsilon_n$ also can appear as other gradients. Appendix A shows how Eq. (26) produces the well-known diffusion Eqs. (1)–(4). The next section shows that $\nabla\Upsilon_k$ are the conjugate force vectors $\mathbf{X_k}$ in the NET–DPE approach.

2.4. Comparison with NET theory

The NET Eq. (7) adapted for conservative forces can be rewritten without additional assumptions as

$$\sigma = -\frac{\mathbf{Q}\cdot\nabla T}{T^2} - k\sum_{k=1}^{n} \hat{\mathbf{J}}_\mathbf{k}\cdot\left[\nabla \ln\left(\frac{f_k}{T}\right) + \left(1 + \frac{\varphi_k}{kT}\right)\frac{\nabla T}{T}\right] + \cdots, \tag{27}$$

where $f_k = e^{(\mu_k^\circ + \varphi_k)/kT}$. Proceeding in the same manner as de Groot and Mazur [23] in obtaining Eq. (8), one can amend the definition of the entropy flux to

$$\frac{\mathbf{Q}'}{T} = \frac{\mathbf{Q}}{T} - k\sum_k \left(1 + \frac{\varphi_k}{kT}\right)\hat{\mathbf{J}}_\mathbf{k}$$

in order to convert Eq. (27) to

$$\sigma = -\frac{\mathbf{Q}'\cdot\nabla T}{T^2} - k\sum_{k=1}^{n} \hat{\mathbf{J}}_\mathbf{k}\cdot\left[\nabla \ln\left(\frac{f_k}{kT}\right)\right] + \cdots, \tag{28}$$

where the conjugate force vectors appear in brackets. Near thermodynamic equilibrium and in the absence of chemical reactions, it follows that the con-

jugate force vectors in Eq. (28) also can be written as

$$\mathbf{X_k} = \nabla \ln\left(\frac{f_k b_k}{\varkappa \tau_k kT}\right); \tag{29}$$

because $\nabla \ln \tau_n = 0$ near equilibrium, $\nabla \ln b_k = 0$ for a constant molecular size, and $\nabla \ln \varkappa = 0$ since the coordination number is a constant. A comparison of Eqs. (24) and (29) shows that $\nabla \Upsilon_k = \mathbf{X_k}$.

It should be noted that the current LDFT approach, which is for systems that are not necessarily isothermal, does not provide equations for heat flux. Consequently, it is not yet possible to check whether Onsager's reciprocity relations will be obeyed, or whether LDFT correctly predicts the Dufour effect. Nevertheless, the analysis up to Eq. (26) also holds for the isothermal case, which has the same integrating factor for $đ\Gamma_n$ shown in Eq. (23). The examples in the following subsections use the isothermal criterion (as noted) in order to provide physical insight to the property Γ_n.

2.5. Analytical examples of the driving force Γ_n

It is useful to know that the function Υ_k exists with a differential form of Eq. (24), with a relationship to the diffusive flux through Eq. (26), and in agreement with the NET approach with regard to the conjugate force vectors for diffusive flux. However, the objectives are to understand the property Γ_n and to provide Eq. (9). This section provides an analysis of Γ_n.

Combining Eqs. (23) and (24) gives

$$đ\Gamma_n = \frac{\rho_n}{\varkappa \tau_n}\left(1 - \sum_m \rho_m\right) d \ln\left(\frac{f_n b}{\varkappa \tau_n kT}\right) \tag{30}$$

or

$$đ\Gamma_n = \left(1 - \sum_m \rho_m\right)^2 exp\left(-\frac{\varphi_n + \varepsilon_n}{kT}\right) d\left(\frac{f_n b}{\varkappa \tau_n kT}\right), \tag{31}$$

where the latter incorporates the definition of the fugacity, Eq. (25). The following substitution of variables simplifies this problem and, later, gives more insight into the property Γ_n:

$$Y_n = \frac{\left(1 - \sum_m \rho_m\right)^2}{exp\left(\frac{\varphi_n + \varepsilon_n}{kT}\right)} \quad X_n = \frac{\rho_n}{\varkappa \tau_n}\left(1 - \sum_m \rho_m\right), \tag{32}$$

where Y_n is a dimensionless ratio representing repulsive to attractive intermolecular interactions for species n, and X_n represents the impingement rate of

molecules n onto vacancies at each of the $\varkappa$ adjacent lattice sites. Using this substitution, Eqs. (30) and (31) can be rewritten as

$$\bar{d}\Gamma_n = Y_n d\left(\frac{X_n}{Y_n}\right), \tag{33}$$

where the ratio X_n/Y_n equals $f_n b/\varkappa\tau_n kT$.

We chose this substitution because, for processes of constant Y_n, it immediately is evident that $\bar{d}\Gamma_n = dX_n$ and $\hat{J}_n = -\frac{\lambda}{A}\nabla X_n$ where λ/A is always constant; i.e., the diffusive flux is driven by the gradient of the impingement rate onto vacancies, at least for constant Y_n processes – this is the case for pure or multicomponent systems of interacting molecules under isothermal conditions with constant ∇f_n and $\tau_n = \tau_n(T)$. Even after the substitution, however, the second partial derivatives of Γ_n with respect to X_n and Y_n are not interchangeable – integration of $\bar{d}\Gamma_n$ generally requires a "path" between two limits. The following sections provide a few reasonable "paths" that characterize Γ_n.

Path 1. Near-ideal gases

For pure near-ideal gases (NIG) and near-ideal gas mixtures (NIGM), $Y_n = 1$ and $X_n = \frac{\rho_n}{\varkappa\tau_n}$, because intermolecular interaction energies are small and the insertion probability approaches unity; this also is evident from the high-temperature and low-density limit of Eq. (32), which has the insertion probability $(1 - \sum_m \rho_m)$. Thus, integration of Eq. (33) gives $\Gamma_n^{NIG} = \Gamma_n^{NIGM} = \Gamma_n^* + \frac{\rho_n}{\varkappa\tau_n}$, where the term Γ_n^* is independent of X_n. Since there is no diffusion of species n when $\rho_n = 0$, it is reasonable that the constant $\Gamma_n^* = 0$, giving

$$\Gamma_n^{NIG} = \Gamma_n^{NIGM} = \frac{\rho_n}{\varkappa\tau_n} = \frac{4}{\varkappa}\left(\lambda^2 \frac{P_n}{\sqrt{2\pi M_n kT}}\right), \tag{34}$$

which makes use of $\rho_n = P_n\lambda^3/kT$ and $\tau_n = \lambda\sqrt{\pi M_n/8kT}$; where P_n is the partial pressure, and M_n is the molecular mass of species n. Thus, Γ_n^{NIG} and Γ_n^{NIGM} represent the impingement rate of molecules on their surroundings – recall the Hertz–Knudsen formula $P_n/\sqrt{2\pi M_n kT}$ for the molecular flux to a surface in units of $1/(area \cdot time)$. Appendix B explains why this section considers near-ideal gases rather than true ideal gases.

Path 2. Rigid spheres (one component, isothermal process)

For a one-component system of rigid spheres under isothermal conditions, $Y = (1-\rho)^2$ and $X = \rho(1-\rho)/\varkappa\tau$. Assuming that $\tau = \tau(T)$, where M is the

molecular mass, allows integration of Eq. (33) to give $\Gamma^{RS} = \Gamma^{RS*}(T) + \frac{\rho}{\varkappa\tau}$, where $\Gamma^{RS*}(T)$ is the constant of integration. For all temperatures, however, the low-density limit requires $\Gamma^{RS*} = 0$, which is reinforced by the notion that the rate of impingement is zero when there are no molecules. Consequently,

$$\Gamma^{RS} = \frac{\rho}{\varkappa\tau} = \frac{4}{\varkappa}\left[\frac{b/\sigma}{(1 + Pb/kT)}\frac{P}{\sqrt{2\pi MkT}}\right], \tag{35}$$

which makes use of the approximations $P(v - b)/kT = 1$ and $\tau = \sigma\sqrt{\pi M/8kT}$, where σ is the sphere diameter. The term $(1 + Pb/kT)$ in Eq. (35) is a correction to the Hertz–Knudsen formula; for a given pressure, fewer molecules impinge on a surface in a period of time for rigid spheres than for a near-ideal gas.

Path 3. Rigid sphere mixture (isothermal process at constant total density)

For an isothermal, multicomponent rigid-sphere system at a constant total density, $Y_n = (1 - \sum_m \rho_m)^2$ and $X_n = \rho_n(1 - \sum_m \rho_m)/\varkappa\tau_n$. Assuming that $\tau_n = \tau_n(T)$ allows integration of Eq. (33) to give $\Gamma_n^{RS} = \Gamma_n^{RS*}(T, \rho_{m\neq n}) + \frac{\rho_n}{\varkappa\tau_n}$, where $\Gamma_n^{RS*}(T, \rho_{m\neq n})$ is the constant of integration that may depend on temperature and all densities except ρ_n. For all temperatures and densities of other species, the low ρ_n limit requires that $\Gamma_n^{RSM*} = 0$, which is reinforced by the notion that the diffusive flux of species n is zero when there are no molecules of species n. Consequently,

$$\begin{aligned}\Gamma_n^{RSM} &= \frac{\rho_n\left(1 - \sum_m \rho_m\right)}{\varkappa\tau_n} \\ &= \frac{4}{\varkappa}\left(1 - \sum_m \rho_m\right)\left[\frac{b_n/\sigma_n}{\left(1 + \frac{P}{kT}\sum_m \omega_m b_m\right)}\frac{\omega_n P}{\sqrt{2\pi M_n kT}}\right],\end{aligned} \tag{36}$$

which makes use of the approximations $P(v - b)/kT = 1$, $b = \sum_m \omega_m b_m$, and $\tau_n = \sigma_n\sqrt{\pi M_n/8kT}$; the term ω_n is the molecular fraction of species n. This result represents the impingement rate of species n onto surrounding vacancies.

A major difference among Eqs. (34)–(36) is the appearance of the insertion probability $(1 - \sum_m \rho_m)$ in Eq. (36). This is a consequence of the constant total-density criterion of Path 3. Equation (36) does not reduce to Eq. (35) in

the limit as the number of species decreases to one because Path 3 is restricted to a constant total density whereas Path 2 is not. This is explained further in Appendix C, and it is an example of how Γ_n depends on the probability of there being *malleable constituents* in the surroundings (i.e., vacancies and molecules of species whose density gradients can be influenced by diffusion).

Path 4. Lattice fluid (one component, isothermal process)

For a one-component lattice fluid with nearest-neighbor interactions and no external fields, $Y = (1-\rho)^2 \exp(-\varkappa\varepsilon\rho/kT)$ and $X = \rho(1-\rho)/\varkappa\tau$. Assuming that $\tau = \tau(T)$ allows integration of Eq. (33),

$$\Gamma = \frac{1}{\varkappa\tau}\left[\rho + \frac{\varkappa\varepsilon}{kT}\left(\frac{\rho^2}{2} - \frac{\rho^3}{3}\right)\right], \tag{37}$$

which makes use of the limit $\Gamma(\rho = 0) = 0$. When there are no attractions ($\varepsilon = 0$), Eq. (37) gives the one-component rigid-sphere result $\rho/\varkappa\tau$ in Eq. (35). This result does not have the insertion probability that appears in the numerator of Eq. (36) because this path does not have a constant total-density criterion. The lack of an insertion probability is explained further in Appendix C and it is an example of how Γ_n is not a simple function.

As a test of Eq. (37), combination with Eq. (9) under the restrictions of this "path" gives

$$\hat{J} = -\frac{\lambda^2}{\varkappa\tau}\left[1 + (1-\rho)\frac{\varkappa\varepsilon\rho}{kT}\right]\nabla C, \tag{38}$$

where $C = \rho/\lambda^3$ and the area through which diffusive flow occurs is $A = \lambda^2$. This is the proposed diffusion equation that gives figures 2–6 in reference [50]. When $T = T_c$ and $\rho = \frac{1}{2}$, the bracketed term in Eq. (38) equals zero – this is the correct result at the critical point [2]. Thus, the new driving force provided in Eq. (37) gives a vanishing diffusive flux at the critical point, i.e., it gives item (f) as promised in the introduction. Furthermore, the bracketed term has negative values for states below the spinodal function on a $T-\rho$ phase diagram; i.e., diffusion occurs against concentration gradients in the spinodal decomposition process.

The driving force in Eq. (37) also gives the fluxes and non-equilibrium phase behavior in figures 2–6 of reference [50], which yields the non-equilibrium density profiles in the x dimension by solving a steady-state material balance equation to give the profile

$$\frac{x}{L} = \frac{\rho - \rho_0 + \frac{\varkappa\varepsilon}{kT}\left(\frac{\rho^2}{2} - \frac{\rho^3}{3}\right) - \frac{\varkappa\varepsilon}{kT}\left(\frac{\rho_0^2}{2} - \frac{\rho_0^3}{3}\right)}{\rho_L - \rho_0 + \frac{\varkappa\varepsilon}{kT}\left(\frac{\rho_L^2}{2} - \frac{\rho_L^3}{3}\right) - \frac{\varkappa\varepsilon}{kT}\left(\frac{\rho_0^2}{2} - \frac{\rho_0^3}{3}\right)}.$$

It now is evident that this profile from reference [50] is an expression for the linearity of the driving force in Eq. (37); i.e., it is equivalent to

$$\Gamma(x) = \left[\frac{\Gamma(L) - \Gamma(0)}{L}\right] x + \Gamma(0).$$

The discussion in this paper provides a very simple physical interpretation of the driving force in Eq. (37).

2.6. Graphical analysis of the driving force Γ_n

Equations (34)–(36) show that Γ_n represents a rate of impingement of molecules onto malleable constituents in the surroundings, at least for near-ideal gases, rigid spheres, and constant total-density rigid-sphere mixtures. This is not obvious for the lattice fluid undergoing Path 4, i.e., Eq. (37) appears to be an impingement rate only in the low-density limit. For a different perspective of Γ_n, this section provides a graphical analysis by using Eq. (33), which shows that Γ_n is the area under the "path" in Y_n versus X_n/Y_n space. Recall from Eq. (32) that Y_n is a ratio of intermolecular repulsions to attractions and that $X_n/Y_n = f_n b/\varkappa\tau_n kT$.

Figure 1 shows examples of Paths 1–4 in Y_n versus X_n/Y_n space. At low values of X_n/Y_n, the area $\Gamma_n^4 > \Gamma_n^1 > \Gamma_n^2 > \Gamma_n^3$. In going from Path 1 to 2,

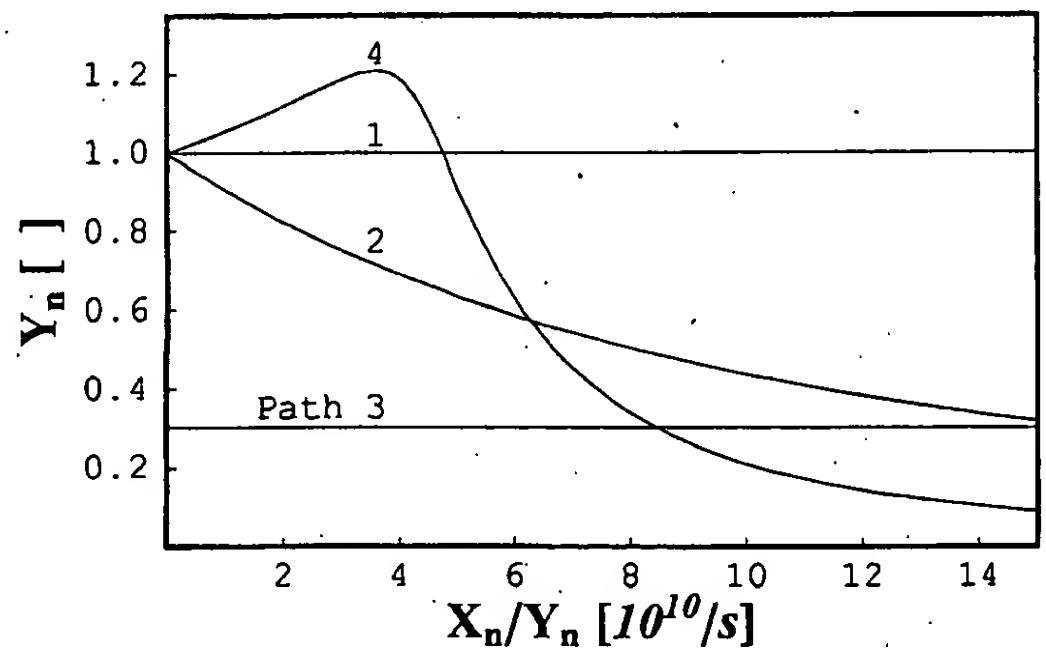

Figure 1 Isotherms in Y_n versus X_n/Y_n space. Paths: (1) pure near-ideal gas and near-ideal gas mixture, (2) rigid spheres, (3) rigid sphere mixture at constant total density, and (4) lattice fluid. The following parameters were chosen arbitrarily: $\tau_n = 8.5 \times 10^{-13} s$ and $\varkappa = 6$ for all paths; $\sum_m \rho_m = 0.45$ for Path 3; and $\varepsilon/kT = 0.5$ for Path 4. Areas under the curves equal the property Γ_n, which is the rate of impingement of molecules on their surroundings at least for Paths 1–3 as described in Eqs. (33)–(36).

the decrease in area is caused by the rigid-sphere repulsion of species n; in going from Path 2 to 3, the decrease is caused by the rigid-sphere repulsion from all the species in the mixture – the area under Path 3 is 65% of the area under Path 1 due to the insertion probability $0.65 = (1 - \sum_m \rho_m)$. On the other hand, in going from Path 1 to 4, the increase in area at low X_n/Y_n is caused by a greater contribution from attractive interactions than from repulsive interactions, which dominate at higher values of X_n/Y_n for the lattice fluid. If this low X_n/Y_n behavior appears counterintuitive, consider that in the low X_n/Y_n range this lattice fluid has a greater pressure than an ideal gas with the same fugacity; i.e., $(f/P) < 1$ for the lattice fluid at low density, whereas $f = P$ for an ideal gas. Therefore, at low X_n/Y_n, the rate of impingement of the lattice fluid is greater than that of the ideal gas.

Path 4 is the only path in Figure 1 that does not have monotonic behavior and it is the "path" used in reference [50]; therefore, it is worth investigating it further. Figure 2 shows more examples of lattice fluids undergoing Path 4. For fluids that are below their critical temperatures, the path can be multivalued at a particular value of X_n/Y_n – this is not the case for fluids that are above their critical temperatures. Figure 3 describes the meaning of this nontrivial behavior of subcritical fluids undergoing Path 4 for a particular value of ε/kT.

For interpreting Figure 3, it may be useful to consider an isothermal lattice fluid in a piston-cylinder system. At vapor-liquid equilibrium (VLE) there is no diffusive flux; this occurs at the intersection points 2 and 8 in Figure 3,

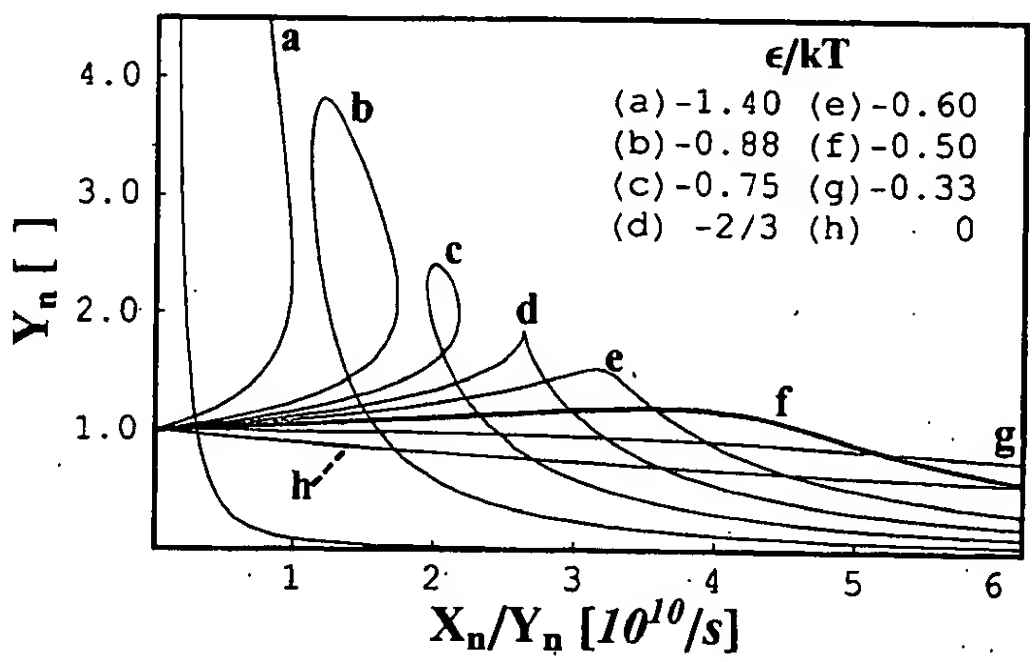

Figure 2 Lattice fluids with different values of ε/kT undergoing Path 4 in Y_n versus X_n/Y_n space. For all data, $\tau_n = 8.5 \times 10^{-13} s$ and $z = 6$. The bolded curve (f) is the Path 4 curve shown in Figure 1. The fluid giving curve (d) has an $\varepsilon/kT = -2/3$, which represents the critical temperature; the maximum along this curve occurs exactly at the critical point. The fluids giving curves (a)–(c) are below their critical temperatures, whereas the fluids giving curves (e)–(h) are above their critical temperatures.

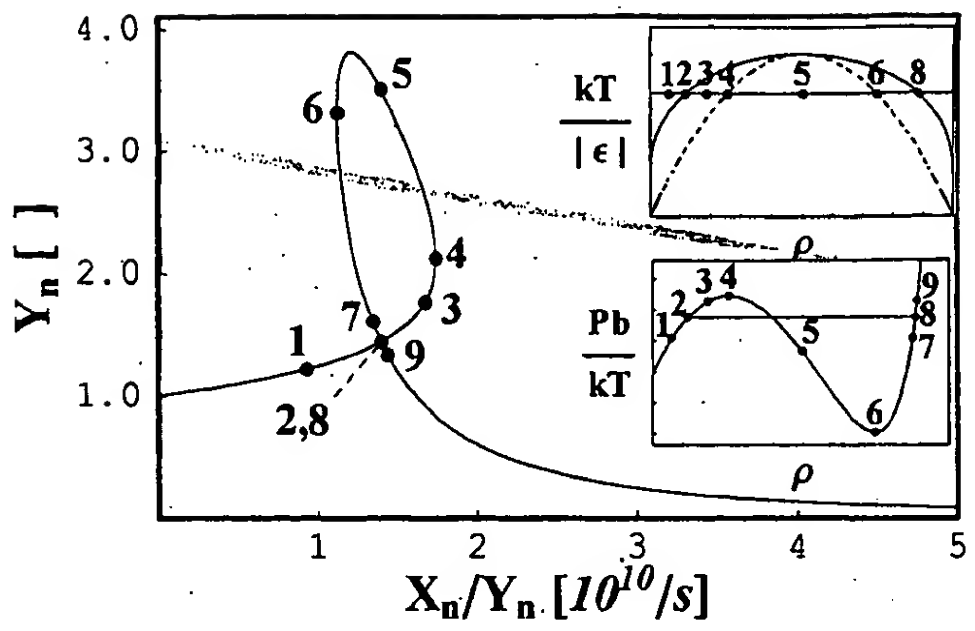

Figure 3 Subcritical lattice fluid undergoing Path 4 in Y_n versus X_n/Y_n space. For this path, $\tau_n = 8.5 \times 10^{-13} s$, $\varepsilon/kT = -0.88$, and $\varkappa = 6$; it is exactly the same as the corresponding curve in Figure 2. Subplots show the locations of points on the phase diagrams. In the $kT/|\varepsilon|$ versus ρ diagram, the solid curve is the binodal and the dashed curve is the spinodal; the critical point is at $kT/|\varepsilon| = 1.5$ and $\rho = 0.5$. Points 2 and 8 are at the same location in Y_n versus X_n/Y_n space, but not on the phase diagrams.

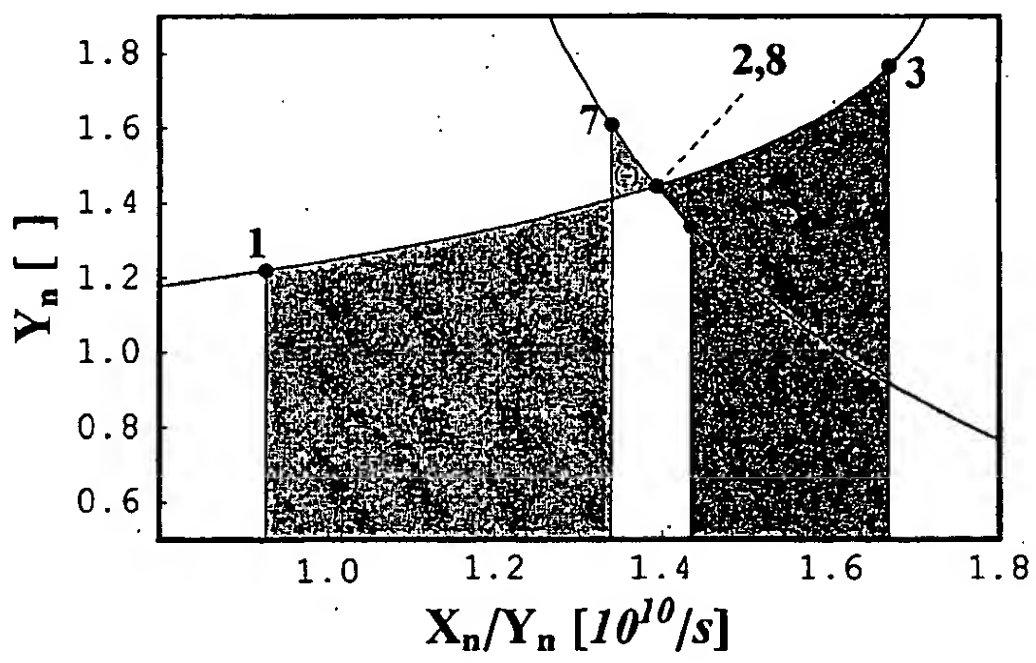

Figure 4 Illustration of the differences $\Gamma_n^{liq}(7) - \Gamma_n^{vap}(1)$ and $\Gamma_n^{vap}(3) - \Gamma_n^{liq}(9)$ for the lattice fluid described in Figure 3. When the system is pressurized to the metastable state represented by points 3 and 9, diffusive flux occurs from the vapor to the liquid phase; for the metastable state represented by points 1 and 7, diffusive flux occurs from the liquid to the vapor. When integrating from point 1 to 7, the area mostly is positive (+) except for the small region labeled negative (−); in the integration from point 8 to point 7, $d(X_n/Y_n) < 0$.

which shows that the areas under the "path" to these points are the same, i.e., the driving forces $\Gamma_n^{vap}(2) = \Gamma_n^{liq}(8)$. When this system is pressurized slightly to the metastable state represented by points 3 and 9, diffusive flux occurs from the vapor to the liquid phase because $\Gamma_n^{vap}(3) > \Gamma_n^{liq}(9)$; this reduces the pressure, returning the system to VLE. On the other hand, if the system originally in VLE is brought to the metastable state represented by points 1 and 7, a diffusive flux would occur from the liquid phase to the vapor phase because $\Gamma_n^{liq}(7) > \Gamma_n^{vap}(1)$. Figure 4 shades both differences $\Gamma_n^{vap}(3) - \Gamma_n^{liq}(9)$

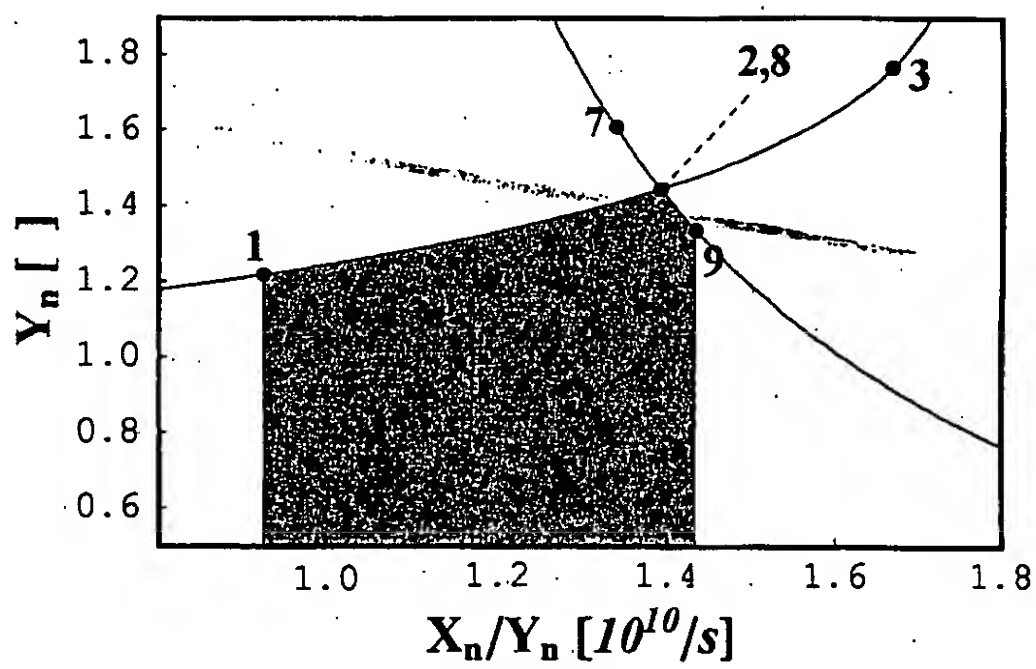

Figure 5 Illustration of the difference $\Gamma_n^{\text{liq}}(9) - \Gamma_n^{\text{vap}}(1) > 0$; for the lattice fluid described in Figure 3. This fluid encounters a vapor–liquid phase transition, as described in reference [50], in which diffusive flux occurs from the liquid to the vapor phase. Points 1 and 9 are the boundary conditions, which are in the stable one-phase region of the phase diagram.

and $\Gamma_n^{\text{liq}}(7) - \Gamma_n^{\text{vap}}(1)$; note that integration from point 8 toward the points 7 and 6 produces negative areas, i.e., $\Gamma_n^{\text{liq}}(8) > \Gamma_n^{\text{liq}}(7) > \Gamma_n^{\text{liq}}(6)$.

In figure 6 of reference [50], two isothermal diffusion processes encountering a vapor-liquid phase transition are summarized: diffusive flux occurs (i) from the liquid to the vapor phase when the boundary conditions represent fluids in the stable one-phase region, and (ii) from the vapor to the liquid phase when the boundary conditions represent fluids in the metastable regions. An example of case (i) is a two phase system at points 1 and 9 in Figure 3; diffusive flux occurs from the liquid to the vapor because $\Gamma_n^{\text{liq}}(9) > \Gamma_n^{\text{vap}}(1)$ as shaded in Figure 5. On the other hand, an example of case (ii) is a two-phase system at points 3 and 7 in Figure 3; diffusive flux occurs from the vapor to the liquid in this case because $\Gamma_n^{\text{vap}}(3) > \Gamma_n^{\text{liq}}(7)$ as shaded in Figure 6.

As a final example, consider the phenomenon of spinodal decomposition. When a uniform supercritical fluid is quenched to temperature below the spinodal function in the subplot of Figure 3, the system immediately becomes unstable; a small fluctuation in ρ due to thermal motion causes decomposition of this system into two stable phases. Figure 7 illustrates the driving force behind this phenomenon for a lattice fluid originally uniform at $\rho = 0.5$ and quenched to $kT/|\varepsilon| = 0.714$ (the critical point occurs at $kT/|\varepsilon| = 1.5$). In this figure, $\Delta\rho$ is a small fluctuation in the density, which can be caused by thermal motion and which creates the driving force difference $\Gamma(\rho - \Delta\rho) - \Gamma(\rho + \Delta\rho)$. Note that integration along the path in the negative X_n/Y_n direction gives a negative value for the area; therefore, diffusion occurs from regions of lower density to regions of higher density because $\Gamma(\rho - \Delta\rho) > \Gamma(\rho + \Delta\rho)$. This enlarges the density fluctuation $\Delta\rho$ and, consequently, the difference $\Gamma(\rho - \Delta\rho) - \Gamma(\rho + \Delta\rho)$, accelerating the decomposition.

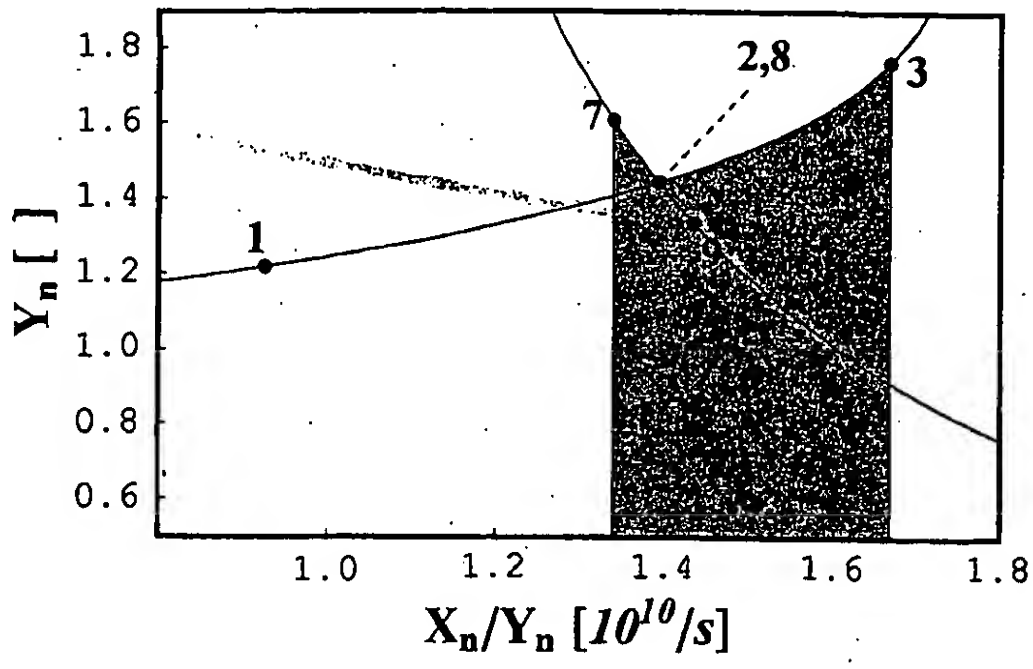

Figure 6 Illustration of the differences $\Gamma_n^{vap}(3) - \Gamma_n^{liq}(7) > 0$; for the lattice fluid described in Figure 3. This fluid encounters a vapor–liquid phase transition, as described in reference [50], in which diffusive flux occurs from the vapor to the liquid phase. Points 3 and 7 are the boundary conditions, which are in the metastable regions of the phase diagram.

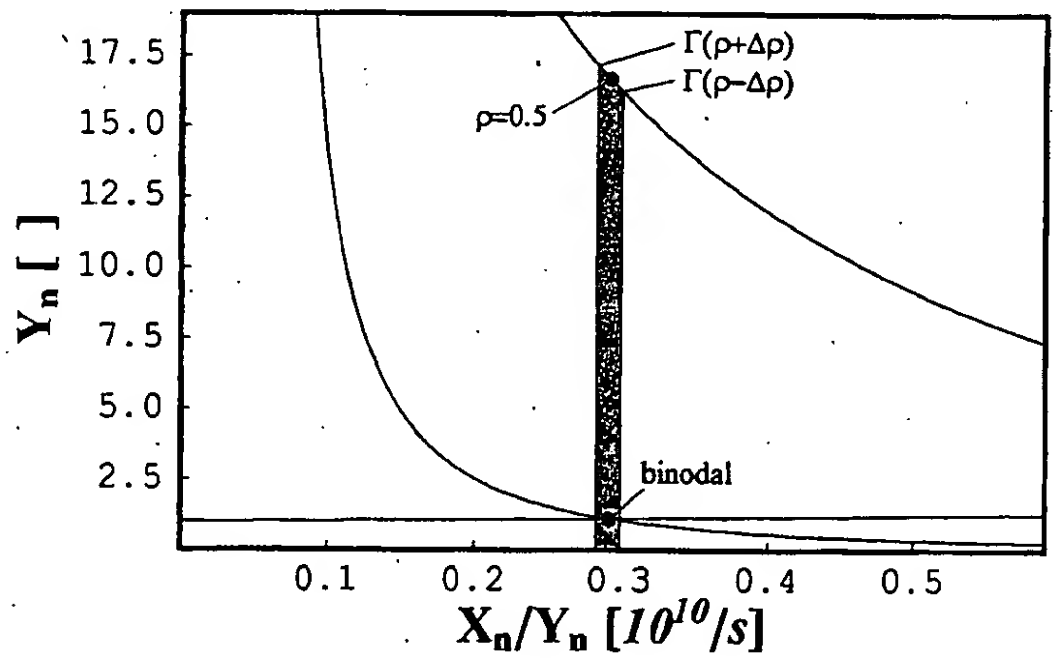

Figure 7 Driving force for spinodal decomposition of a lattice fluid originally uniform at $\rho = 0.5$ that is quenched from supercritical temperature to a temperature $kT/|\varepsilon| = 0.714$ that is below the spinodal function (the critical temperature is $kT/|\varepsilon| = 1.5$). The driving force is the area $\Gamma_n(\rho - \Delta\rho) - \Gamma_n(\rho + \Delta\rho) > 0$, where $\Delta\rho$ is a small fluctuation in the density; diffusion occurs from lower to higher densities, enlarging the fluctuation and accelerating the decomposition.

3. Discussion

Numerous equations have been used to model diffusive flux, but none of these equations generally have a linear relationship between the diffusive flux and the gradient; the coefficients generally depend on the state variables, which usually depend on position and time. This is a mathematical consequence of diffusion's path-dependence. The diffusive flux depends on more than just the difference in the state variables, much like how the heat flux in Clausius's theorem depends on the integrating factor $1/T$ in addition to the difference in

the entropy. Since diffusion is analogous to heat transfer, an integrating factor exists and relates the diffusive flux to a difference in state variables (e.g., to a difference in chemical potential or fugacity). In the LDFT framework, this is summarized by Eq. (26), which uses the integrating factor that multiplies $d\Gamma_n$ in Eq. (23); the chemical potential gradient would arise from the gradient in Eq. (26) by imposing the restrictions of an isothermal and isobaric process in which $\tau_n = \tau_n(T)$.

If one integrating factor exists, however, there exist an infinite number of integrating factors that can have various forms. For example, consider Eq. (31), which shows that $e^{(\varphi_n+\varepsilon_n)/kT}/(1-\sum_m \rho_m)^2$ also is a valid integrating factor in addition to that in Eq. (30). This highlights a fundamental problem for diffusion: the driving force for the diffusive flux can appear to be a variety of gradients. For example, both ∇f_n and $\nabla \ln f_n$ can appear to be driving forces; the latter is equivalent to $\frac{1}{kT}\nabla\mu_n$ for an isothermal and isobaric system. Although the conjugate gradient may change due to the choice of integrating factor as demonstrated by Eqs. (30) and (31), the gradient $\nabla\Gamma_n$ remains independent of the choice of integrating factors. Furthermore, $\nabla\Gamma_n$ always is linearly proportional to the diffusive flux, as shown in Eq. (9). Therefore, we propose that $\nabla\Gamma_n$ is a more general thermodynamic driving force for diffusion. The challenge is determining what Γ_n represents physically.

Equations (34)–(36) and Appendix C show that Γ_n appears as the impingement rate of n molecules onto the malleable constituents in the surroundings; at least for near-ideal gases, rigid spheres, and constant total-density rigid-sphere mixtures. This is reassuring because kinetic theory approaches for gas diffusion begin with defining the flux as the difference in the rate of impingement [55]; these approaches are for constant total-density systems in the dilute limit, which has an insertion probability of unity – the probability of encountering a malleable constituent is unity. For the lattice fluid undergoing Path 4, however, the impingement rate is not obvious in Eq. (37) outside of the low-density limit. This is not necessarily a mistake – the partial derivative of Γ with respect to ρ gives the diffusive flux in Eq. (38), predicting the correct (vanishing flux) behavior at the critical point and the non-equilibrium phase transitions in reference [50]. Of course, this mean-field result is qualitative, and it would need to be extended for quantitative accuracy [47].

The property Γ_n can be difficult to interpret because it is not a state function and it is not apparent unless a "path" is specified. The following is one very simple physical interpretation of Γ that clarifies why the impingement rate is not obvious in Eq. (37) outside of the low-density limit. First consider the one-dimensional case of Eq. (38),

$$\hat{j}^x = -\frac{2\lambda^2}{\varkappa\tau kT}\left(\frac{kT}{2} - \Delta U^{mix}\right)\left.\frac{\partial C}{\partial x}\right|_{y,z},$$

where $\Delta U^{mix} = -\varkappa\varepsilon\rho(1-\rho)/2$ and is the change in configurational energy per site upon mixing for regular solutions of vacancies and molecules with nearest-neighbor interactions, and the term $kT/2$ is the x component of the mean kinetic energy per molecule. The term ΔU^{mix} is positive for intermolecular attractions, acting as an energetic penalty for the mixing of molecules and vacancies, and contributing to vapor–liquid phase transitions at low enough temperatures. Therefore, when molecules' kinetic energy in the x direction exceeds the energetic penalty for interchanging with vacancies, diffusion occurs down the concentration gradient in the x direction (i.e., molecules move toward the vacancies). If ΔU^{mix} is greater in magnitude than the mean kinetic energy, diffusion occurs against this concentration gradient. To make the connection to the property Γ, consider the case $kT/2 > \Delta U^{mix}$. When noninteracting molecules impinge on an imaginary surface perpendicular to the direction of motion, on average they carry $kT/2$ through the surface in a short period of time. When intermolecular attraction occurs, the amount of internal energy carried through this imaginary surface is less than $kT/2$, as there is a toll ΔU^{mix} for moving into a vacant site. The dimensionless amount of internal energy per site that passes through the surface in a period of time is

$$\Gamma = \frac{\rho}{\varkappa\tau}\frac{\int_0^\rho\left(\frac{kT}{2} - \Delta U^{mix}\right)d\rho}{\frac{kT}{2}\int_0^\rho d\rho} = \frac{1}{\varkappa\tau}\left[\rho + \frac{\varkappa\varepsilon}{kT}\left(\frac{\rho^2}{2} - \frac{\rho^3}{3}\right)\right].$$

Thus, Γ can be interpreted as a rate of dimensionless internal energy that is available per site for molecular translation in each of $\varkappa$ directions. The product ΓkT appears to be the available power for molecular translation in the $\pm x$ directions. For near-ideal gas molecules and noninteracting rigid spheres ($\Delta U^{mix} = 0$), this rate of dimensionless energy appears as the rate of impingement in each of $\varkappa$ directions:

$$\Gamma = \frac{\rho}{\varkappa\tau}\frac{kT/2}{kT/2} = \frac{\rho}{\varkappa\tau}.$$

This is one interpretation of Path 4.

There can be an infinite number of paths between two thermodynamic states. Many isothermal paths involving steady-state diffusion of interacting species have constant fugacity gradients; even processes involving mixtures of interacting molecules in a strong external field exhibit nearly linear fugacity profiles in the dimension of the diffusive flux [52]. Such processes have constant values of Y_n in Eqs. (32) and (33). For these cases $d\Gamma_n = dX_n$, i.e., the diffu-

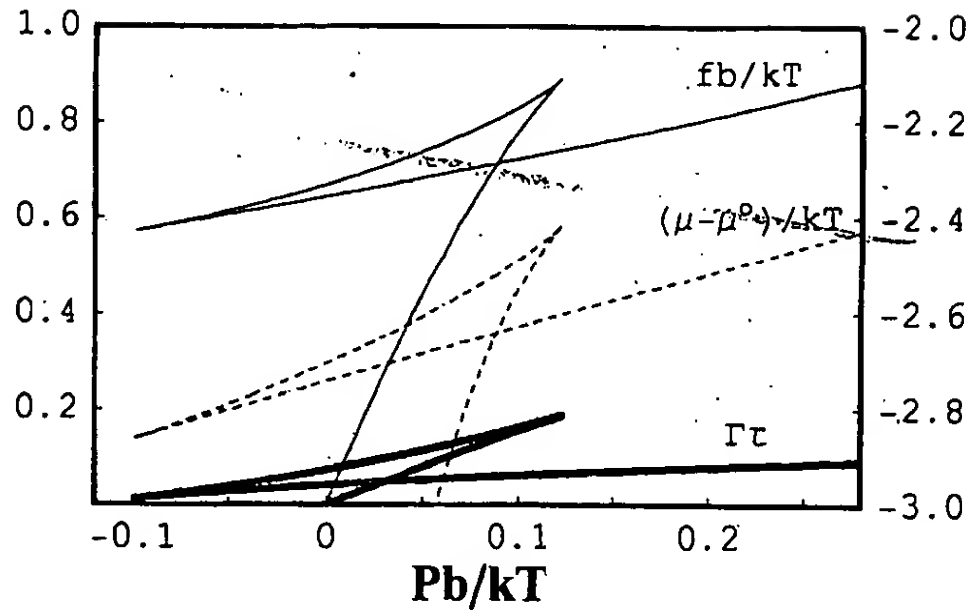

Figure 8 Comparison of Γ, μ, and f for the lattice fluid with $\varepsilon/kT = -0.88$ and $\varkappa = 6$; all are shown in dimensionless form versus the dimensionless pressure. A dimensionless pressure of 0.100 is equivalent to 10.5 MPa for argon at a temperature of 300 K. Values of the dimensionless chemical potential appear on the right axis in excess of the ideal gas reference potential μ^o. Values of the dimensionless Γ and f appear on the left axis.

sive flux is driven by the gradient of the impingement rate onto vacancies. Figure 8 compares Γ_n, μ_n, and f_n for a lattice fluid undergoing Path 4. These properties exhibit very similar behavior; therefore, it is not surprising that Γ_n can be mistaken for an energy density such as the chemical potential or the fugacity. We hope that the skeptical reader would at least recognize that Eqs. (3) and (4) are identical and that the coefficient to ∇f_n is constant more often than the coefficient to $\nabla \mu_n$. This occurs mostly because it is more probable to have a uniform C_{tot} than a uniform C_n when there is diffusive flux of species n.

Equation (9) is a linear law describing diffusion; the linear relationship between the diffusive flux and the gradient remains in the presence of gradients in ρ_n, ρ_m, φ_n, μ_n, f_n, T, and τ_n. The gradient in Eq. (9) transforms into a well-recognized gradient (e.g., the chemical potential gradient) only when particular properties are uniform, as shown in Appendix A. If a sufficient number of properties are uniform, the resultant diffusion equation can have a linear diffusive flux with respect to any one of several different gradients.

4. Conclusions

The LDFT framework was used to formulate a linear diffusion equation that has a constant coefficient even in the presence of gradients in all the state variables. It is proposed that the gradient in this equation is the driving force for diffusion. This driving force is related to the gradient of state variables (e.g., to the chemical potential gradient) through integrating factors, much like in Clausius's theorem, which relates the heat flux to the difference in entropy through the integrating factor $1/T$. At constant temperature, for near-ideal gases, rigid spheres, and constant total-density rigid-sphere mixtures,

the driving force for diffusion appears to be the gradient of the impingement rate of molecules on malleable constituents of the surroundings. For the lattice fluid with nearest-neighbor attractions, the driving force appears to be the gradient of the impingement rate at low densities; but it deviates outside of this limit, appearing more like a rate of dimensionless internal energy available for molecular translation – this rate of dimensionless internal energy equals the rate of impingement when the configurational energy of mixing molecules and vacancies is zero. This paper shows that the proposed driving force gives the well-known diffusion equations, a vanishing diffusive flux at the critical point, and agreement with the theory of non-equilibrium thermodynamics. Furthermore, this paper uses this driving force to explore various diffusion equations, finding that the diffusive flux is linear more often with the fugacity gradient than with the chemical potential gradient because, when species n diffuses, it is more probable to have a constant total-density than a constant density of species n.

Appendix A: Uniform properties produce the well-known diffusion equations

Equations (1)–(4) are simplifications of a more general equation for the diffusive flux. Fickian behavior (with a constant diffusivity) is observed only when a sufficient number of state variables are uniform. This section demonstrates this by showing that Eq. (26) reduces to the well-known diffusion equations.

For isothermal and isobaric systems in which $\tau_n = \tau_n(T)$, Eq. (26) becomes

$$\hat{J}_n = -\frac{\lambda}{A}\nabla\Gamma_n = -\frac{\lambda^2}{\varkappa\tau_n}\frac{C_n}{kT}\left(1-\sum_m \rho_m\right)\nabla\mu_n, \tag{A.1}$$

which is Eq. (4) in the LDFT framework. On the other hand, for isothermal systems with $\tau_n = \tau_n(T)$, Eq. (26) has the form of

$$\hat{J}_n = -\frac{\lambda}{A}\nabla\Gamma_n = -\frac{\lambda^2}{\varkappa\tau_n kT}\left(1-\sum_m \rho_m\right)^2 exp\left(-\frac{\varphi_n+\varepsilon_n}{kT}\right)\nabla f_n, \tag{A.2}$$

which is Eq. (3). Equation (A.2) simplifies further when the fugacity coefficient ϕ_n is constant,

$$\hat{J}_n = -\frac{\lambda}{A}\nabla\Gamma_n = -\frac{\lambda^2}{\varkappa\tau_n kT}\left(1-\sum_m \rho_m\right)^2 exp\left(-\frac{\varphi_n+\varepsilon_n}{kT}\right)\phi_n\nabla P_n, \tag{A.3}$$

which is Eq. (2). Lastly, for isothermal systems with $\tau_n = \tau_n(T)$ and the additional restrictions of a constant total density and of no gradients in φ_n and ε_n,

Eq. (26) has the form of

$$\hat{J}_n = -\frac{\lambda}{A}\nabla\Gamma_n = -\frac{\lambda^2}{\varkappa\tau_n}\left(1 - \sum_m \rho_m\right)\nabla C_n, \tag{A.4}$$

which is Eq. (1).

Again, it should be noted that these results are for lattice fluids. To make these results more general, the term $(1 - \sum_m \rho_m)$ should be replaced with the insertion probability as shown in reference [50].

Appendix B: Near-ideal gases versus ideal gases

Path 1 describes near-ideal gases, i.e., real gases that experience collisions but which have properties approaching ideal gas behavior characterized by the equation $PV = nRT$. On the other hand, ideal gases are point masses that do not experience collisions and, therefore, pure ideal gases cannot have an average velocity that differs from the mass-averaged velocity; i.e., their diffusion velocity [56] is zero at uniform temperature and mass-averaged velocity:

$$\overline{V}_i = (\bar{v}_i - v_o) = \frac{1}{n_i}\int V_i \Phi_i \mathrm{f}_i^{[0]}\, dV_i, \tag{B.1}$$

where the diffusion velocity $\overline{V}_i$ is the average velocity of i-molecules $\bar{v}_i$ in excess of the mass-averaged velocity v_o, V_i is the particular velocity of an i-molecule with respect to the mass-averaged velocity, n_i is the number of i-molecules per volume, the (Maxwell–Boltzmann) distribution $\mathrm{f}_i^{[0]}$ is the first term in the velocity distribution function in the Boltzmann equation [57], and Φ_i is the perturbation function that gives the first-order perturbation from the Maxwell–Boltzmann distribution. For gases that experience collisions, Φ_i can be evaluated and is related to the collision integral that appears in the diffusivity for pure or binary gases at low density [55]. On the other hand, for an isothermal system of noninteracting point masses with a uniform mass-averaged velocity, $\Phi_i^{IG} = 0$ giving $\overline{V}_i^{IG} = 0$. For this reason, Path 1 considers near-ideal gases, which undergo collisions and have a velocity distribution and, therefore, can have diffusion velocity.

Appendix C: "Malleable constituents" and the insertion probability in Γ_n

The property Γ_n has different forms that depend on the constraints/conditions of the diffusion "path". For example, the insertion probability $(1 - \sum_m \rho_m)$ seems to appear arbitrarily in Eq. (36) but it does not appear in Eqs. (34),

(35), and (37). This section demonstrates that the forms of Γ_n have a common origin; that the reason why the insertion probability appears in Eq. (36) is the same for the lack of an insertion probability in Eqs. (34), (35), and (37); and that Γ_n is not limited to the forms of Eqs. (34)–(37).

Previously, it was stated that Γ_n can appear as the impingement rate onto the malleable constituents in the surroundings. For lack of a better term, we consider malleable constituents to include vacancies and molecules of species whose density gradients can be influenced by diffusion; e.g., a constant-density matrix of a solid membrane does not qualify as a malleable constituent even if the molecules of this matrix wander; this is because the density of the matrix does not respond to penetrants. Similarly, a multicomponent system that is restricted to a constant total density, overall, is considered a matrix that does not respond to individual penetrants within the system. With this as the context, we provide the following illustrative example.

Consider a binary system of identical nonattracting spheres that differ only in their "color". Spheres are labeled "1" and "2" as in the problem of isothermal color counterdiffusion of Weeks–Chandler–Anderson fluids [33, 52]. The density profiles of both species are linear in the absence of external fields, $\rho_n = m_n x + b_n$ where m_n is the slope and b_n is the intercept. For this problem we have

$$\tau_n = \tau(T),\ Y_n = (1-\rho_1-\rho_2)^2, \quad X_n = \frac{\rho_n}{\varkappa\tau}(1-\rho_1-\rho_2).$$

This allows integration of Eq. (33) for an isothermal path,

$$\Gamma_1 = \frac{\rho_1}{\varkappa\tau}\left(1+\frac{m_2}{m_1}\rho_1-\rho_2\right). \tag{C.1}$$

There are at least three interesting cases of Eq. (C.1). First, $\Gamma_1^I = \frac{\rho_1}{\varkappa\tau}(1-\rho_1-\rho_2)$ for equal color counterdiffusion at a constant total density ($m_2 = -m_1$); this is the binary version of the constant total-density rigid-sphere mixture result of Eq. (36) – the probability of having a malleable constituent is the vacancy probability $\rho_v = 1-\rho_1-\rho_2$. Second, $\Gamma_1^{II} = \frac{\rho_1}{\varkappa\tau}(1-\rho_2)$ for diffusion of species 1 through a matrix of species 2 in which $\nabla\rho_2 = m_2 = 0$; note that the insertion probability does not appear explicitly – the probability of having a malleable constituent is the sum $\rho_v + \rho_1 = 1-\rho_2$. Third, $\Gamma_1^{III} = \frac{\rho_1}{\varkappa\tau}$ for diffusion of a pure fluid in which half the molecules arbitrarily are labeled "1" ($m_1 = m_2$ and $\rho_1 = \rho_2$); i.e., $\Gamma^{III} = \frac{\rho}{\varkappa\tau}$ where $\rho = 2\rho_1$ for the pure fluid; this is the rigid sphere result, Eq. (35), as well as the noninteracting lattice fluid result, as can be seen from Eq. (37) – the probability of having a malleable constituent is the sum $\rho_v + \rho = 1$.

Thus, the insertion probability may appear explicitly in Γ_n if it equals the probability of having a malleable constituent. However, if the insertion probability does not appear explicitly, it contributes to the flux and driving flux through the equation of state. To reinforce this last point, consider that Eqs. (34) and (35) give

$$\Gamma^{NIG}(T,\rho) = \Gamma^{RS}(T,\rho)$$

$$\Gamma^{NIG}(T,P) > \Gamma^{RS}(T,P).$$

Acknowledgments

Support by the US Department of Energy, under contract no. DE-FG02-87ER13777, is gratefully acknowledged. D.M. acknowledges Building Service 32BJ Thomas Shortman Training, Scholarship and Safety Fund, for a graduate fellowship. D.M. wishes to acknowledge Professor Robert C. Cammarata (Materials Science and Engineering, Johns Hopkins University), for his influential lectures on thermodynamics of materials.

References

[1] Fick, A.E., On liquid diffusion, Philos. Mag., 10 (1855), 30–39.
[2] Cussler, E.L., Diffusion, Mass Transfer in Fluid Systems, 2nd ed., Cambridge University Press, Cambridge, 1997.
[3] Bird, R.B., Stewart, W.E., Lightfoot, E.N., Transport Phenomena. Wiley, New York, 1960.
[4] Karger, J., Ruthven, D.M., Diffusion in Zeolites and Other Microporous Solids, Wiley, New York, 1992.
[5] Einstein, A., Über die von der molekularkinetischen Theorie der Wärme geforderte Bewegung von in ruhenden Flüssigkeiten suspendierten Teilchen, Ann. Phys., 17 (1905), 549–560.
[6] Mitchell, M.C., Gallo, M., Nenoff, T.M., Computer simulations of adsorption and diffusion for binary mixtures of methane and hydrogen in titanosilicates, J. Chem. Phys., 121 (2004), 1910–1916.
[7] Keffer, D.J., Edwards, B.J., Adhangale, P., Determination of statistically reliable transport diffusivities from molecular dynamics simulation, J. Non-Newtonian Fluid Mech., 120 (2004), 41–53.
[8] Trinh, S., Arce, P., Locke, B.R., Effective diffusivities of point-like molecules in isotropic porous media by Monte Carlo simulation, Transport Porous Med., 38 (2000), 241–259.
[9] Reis, R.A., Silva, F.C., Nobrega, R., Oliveira, J.V., Tavares, F.W., Molecular dynamics simulation data of self-diffusion coefficient for Lennard–Jones chain fluids, Fluid Phase Equilib., 221 (2004), 25–33.

[10] Keffer, D.J., Adhangale, P., The composition dependence of self and transport diffusivities from molecular dynamics simulations, Chem. Eng. J., 100 (2004), 51–69.
[11] Paul, D.R., Yampolskii, Y.P., Polymeric Gas Separation Membranes, CRC Press, Boca Raton, FL, 1994.
[12] Bowen, T.C., Li, S.G., Noble, R.D., Falconer, J.L., Driving force for pervaporation through zeolite membranes, J. Membr. Sci., 225 (2003), 165–176.
[13] Onsager, L., Reciprocal relations in irreversible processes, I., Phys. Rev., 37 (1931), 405–426.
[14] Kizilyalli, M., Corish, J., Metselaar, R., Definitions of terms for diffusion in the solid state – (IUPAC recommendations 1999), Pure Appl. Chem., 71 (1999), 1307–1325.
[15] Darken, L.S., Diffusion, mobility and their interrelation through free energy in binary metallic systems, Trans. AIME, 175 (1948), 184–201.
[16] Onsager, L., Fuoss, R.M., Irreversible processes in electrolytes. Diffusion, conductance, and viscous flow in arbitrary mixtures of strong electrolytes, J. Phys. Chem., 36 (1932), 2689–2778.
[17] Skoulidas, A.I., Sholl, D.S., Direct tests of the Darken approximation for molecular diffusion in zeolites using equilibrium molecular dynamics, J. Phys. Chem. B, 105 (2001), 3151–3154.
[18] Reyes, S.C., Sinfelt, J.H., DeMartin, G.J., Diffusion in porous solids: the parallel contribution of gas and surface diffusion processes in pores extending from the mesoporous region into the microporous region, J. Phys. Chem. B, 104 (2000), 5750–5761.
[19] Baierlein, R., The elusive chemical potential, Am. J. Phys., 69 (2001), 423–434.
[20] Krishna, R., Wesselingh, J.A., Review article number 50 – the Maxwell–Stefan approach to mass transfer, Chem. Eng. Sci., 52 (1997), 861–911.
[21] Demirel, Y., Sandler, S.I., Linear-nonequilibrium thermodynamics theory for coupled heat and mass transport, Int. J. Heat Mass Transfer, 44 (2001), 2439–2451.
[22] Demirel, Y.A., Sandler, S.I., Nonequilibrium thermodynamics in engineering and science, J. Phys. Chem. B, 108 (2004), 31–43.
[23] de Groot, S.R., Mazur, P., Non-Equilibrium Thermodynamics, Dover, New York, 1984.
[24] Lebon, G., Desaive, T., Colinet, P., Thermo-diffusion revisited: a comparative approach between two recent thermodynamic formalisms, J. Non-Equilib. Thermodyn., 29 (2004), 405–415.
[25] Johannessen, E., Kjelstrup, S., Nonlinear flux-force relations and equipartition theorems for the state of minimum entropy production, J. Non-Equilib. Thermodyn., 30 (2005), 129–136.
[26] Bedeaux, D., Standaert, F., Hemmes, K., Kjelstrup, S., Optimization of processes by equipartition, J. Non-Equilib. Thermodyn., 24 (1999), 242–259.
[27] Goldstein, P., Garcia-Colin, L.S., On the validity of the Onsager relations in an inert multiple dilute gas mixture, J. Non-Equilib. Thermodyn., 30 (2005), 173–186.
[28] Porter, D.A., Easterling, K.E., Phase Transformations in Metals and Alloys, 2nd ed., Chapman & Hall, London/New York, 1992.
[29] Matuszak, D., Aranovich, G.L., Donohue, M.D., Lattice density functional theory of molecular diffusion, J. Chem. Phys., 121 (2004), 426–435.

[30] Choi, J.G., Do, D.D., Do, H.D., Surface diffusion of adsorbed molecules in porous media: monolayer, multilayer, and capillary condensation regimes, Ind. Eng. Chem. Res., 40 (2001), 4005–4031.
[31] Lee, K.H., Hwang, S.T., The transport of condensable vapors through a microporous vycor glass membrane, J. Colloid Interf. Sci., 110 (1986), 544–555.
[32] Bae, J.S., Do, D.D., Effects of adsorbed phase on diffusion of subcritical hydrocarbons in activated carbon at low pressures, J. Non-Equilib. Thermodyn., 30 (2005), 1–20.
[33] Frink, L.J.D., Thompson, A., Salinger, A.G., Applying molecular theory to steady-state diffusing systems, J. Chem. Phys., 112 (2000), 7564–7571.
[34] Subramaniam, S., Minimum error Fickian diffusion coefficients for mass diffusion in multicomponent gas mixtures, J. Non-Equilib. Thermodyn., 24 (1999), 1–39.
[35] Scherman, D., Henry, J.P., Effect of drugs on the ATP-induced and pH-gradient-driven monoamine transport by bovine chromaffin granules, Biochem. Pharmacol., 29 (1980), 1883–1890.
[36] Caflisch, C., Zimmerli, B., Hugentobler, G., Meier, P.J., pH gradient driven cholate uptake into rat-liver plasma-membrane vesicles represents nonionic diffusion rather than a carrier mediated process, Gastroenterology, 92 (1987), 1722–1722.
[37] Hirvonen, J., Murtomaki, L., Kontturi, K., Effect of diffusion potential, osmosis and ion-exchange on transdermal drug delivery: theory and experiments, J. Control. Release, 56 (1998), 33–39.
[38] Botre, C., Crescenzi, V.L., Liquori, A.M., Mele, A., Concentration gradient and diffusion potential in colloidal electrolyte solutions, T. Faraday Soc., 55 (1959), 1975–1981.
[39] Merk, H.J., The macroscopic equations for simultaneous heat and mass transfer in isotropic, continuous and closed systems, Appl. Sci. Res., A8 (1959), 73–99.
[40] Aranovich, G.L., Donohue, M.D., A new model for lattice systems, J. Chem. Phys., 105 (1996), 7059–7063.
[41] Aranovich, G.L., Donohue, M.D., New approximate solutions to the Ising problem in three dimensions, Physica A, 242 (1997), 409–422.
[42] Aranovich, G., Donohue, P., Donohue, M., A lattice model for fluids with directional interactions, J. Chem. Phys., 111 (1999), 2050–2059.
[43] Sangwichien, C., Aranovich, G.L., Donohue, M.D., Density functional theory predictions of adsorption isotherms with hysteresis loops, Colloids Surf. A, 206 (2002), 313–320.
[44] Aranovich, G.L., Donohue, M.D., Phase loops in density-functional-theory calculations of adsorption in nanoscale pores, Phys. Rev. E, 60 (1999), 5552–5560.
[45] Aranovich, G.L., Donohue, M.D., Lattice density functional theory predictions of order–disorder phase transitions, J. Chem. Phys., 112 (2000), 2361–2366.
[46] Aranovich, G.L., Donohue, M.D., Modeling self-assembly in molecular fluids, J. Chem. Phys., 116 (2002), 7255–7268.
[47] Aranovich, G.L., Erickson, J.S., Donohue, M.D., Lattice gas 2D/3D equilibria: chemical potentials and adsorption isotherms with correct critical points, J. Chem. Phys., 120 (2004), 5208–5216.
[48] Aranovich, G.L., Donohue, M.D., Theory of multilayer adsorption with correct critical behavior, Langmuir, 19 (2003), 3822–3829.
[49] Matuszak, D., Donohue, M.D., Inversion of multicomponent diffusion equations, Chem. Eng. Sci., 60 (2005), 4359–4367.

[50] Aranovich, G., Donohue, M., Diffusion equation for interacting particles, J. Phys. Chem. B, 109 (2005), 16062–16069.
[51] Giacomin, G., Lebowitz, J.L., Marra, R., Macroscopic evolution of particle systems with short- and long-range interactions, Nonlinearity, 13 (2000), 2143–2162.
[52] Matuszak, D., Aranovich, G.L., Donohue, M.D., Modeling multicomponent diffusion using lattice density functional theory: counterdiffusion in an external field, Phys. Chem. Chem. Phys., 8 (2006), 1663–1674.
[53] Evans, R., Nature of the liquid–vapor interface and other topics in the statistical-mechanics of nonuniform, classical fluids, Adv. Phys., 28 (1979), 143–200.
[54] Adkins, C.J., Equilibrium Thermodynamics, Cambridge University Press, Cambridge, 1983.
[55] Bird, R.B., Stewart, W.E., Lightfoot, E.N., Transport Phenomena, Wiley, New York, 2002.
[56] Hirschfelder, J.O., Curtiss, C.F., Bird, R.B., Molecular Theory of Gases and Liquids, 2nd ed., Wiley, New York, 1965.
[57] Chapman, S., Cowling, T.G., The Mathematical Theory of Non-Uniform Gases, Cambridge University Press, Cambridge, 1939.

Paper received: 2005-08-26
Paper accepted: 2006-02-06

APPENDIX 4

WO 95/15147

Use of L-arginine, L-ornithine, or L-citrulline and topical preparations with these substances

The present invention relates to the use of L-arginine, L-ornithine, and/or L-citrulline and the use of cosmetic and dermatological topical preparations that contain these active ingredients.

The epidermis is rich in nerves and nerve end apparatus such as Vater-Pacini corpuscles, Merkel-neurite complexes, and free nerve endings for feeling pain, cold, heat, and itching.

In people who have sensitive skin or skin that is prone to injury it is therefore possible to observe a neurosensory phenomenon called "stinging" (in English, "sting" means to injure, burn, cause pain). This "sensitive skin" is fundamentally different from "dry skin" that has a thickened and hardened stratum corneum.

Typical reactions when there is "stinging" on sensitive skin are reddening, tension, and burning of the skin, as well as itching.

Itching in the case of atopic skin and itching in the case of skin diseases is also considered a neurosensory phenomenon.

The object of the invention is therefore to provide active substances, and topical preparations having such active substances, that prevent neurosensory phenomena or alleviate such phenomena or provide rapid relief for them after they occur, that is, that are suitable for prophylactic purposes and/or treatment.

"Stinging" phenomena can be considered disorders to be treated cosmetically. In contrast, severe itching, in particular severe itching of the skin that occurs with atopy, can also be called a serious dermatological disturbance.

These objects are attained by the use of one or a plurality of compounds selected from the group of L-arginine, L-ornithine, and L-citrulline or their salts, acid addition salts, esters, or amides, where necessary with the addition of folic acid or its salts and/or one or a plurality of compounds selected from the group of flavins, for prophylactic purposes and/or treatment of neurosensory phenomena.

They are preferably used for prophylactic purposes and/or treating neurosensory phenomena of the skin, in particular "stinging" and atopy (neurodermitis).

The subject-matter of the invention is also the use of cosmetic and dermatological topical preparations that contain the inventive active substances,

for prophylactic purposes and/or for treating the neurosensory phenomena.

One skilled in the art would not be able to foresee that the inventive active substances and that cosmetic or dermatological preparations having active ingredients of arginine, citrulline, ornithine, folic acid, and flavins in accordance with the invention would be excellently suited for prophylactic purposes and treatment of neurosensory phenomena.

Preferred salts of L-arginine, L-ornithine, and L-citrulline are water soluble salts, e.g. sodium, potassium, and ammonia salts. This also applies to the acid addition salts. Suitable acid additional salts are obtained with inorganic and organic acids. Hydrochlorides, sulfates, acetates, caprylates, and citrates are preferred.

Suitable esters of these compounds are e.g. those that are formed with short-chain and medium-chain alcohols, preferably mono-alcohols, but in particular methanol, ethanol, or propanol. The ethylesters are preferred.

Preferred amides are short-chain and medium-chain mono-alkylamides and di-alkylamides.

Alkyls with the aforesaid substituents contain e.g. up to 12 carbon atoms, preferably up to 6 carbon atoms.

Particularly preferred are active substance combinations and topical preparations that contain L-arginine and/or its inventive derivatives.

L-arginine and its derivatives are also distinguished by particularly good skin penetration ability.

The inventive amino acids and/or their derivatives are preferably contained in the inventive cosmetic and dermatological preparations in quantities of 0.01 to 30 wt.%, particularly preferred 0.01 to 10 wt.%, especially 0.1 – 7.5 wt.%, relative to the total preparation. L-arginine, ornithine, and citrulline and their derivatives can be employed individually or in combination; however in this case the preparations then contain particularly preferred L-arginine in quantities of 1 to 10 wt.%, relative to the total preparation.

Particularly suitable salts of folic acids are water-soluble salts, especially sodium, potassium, and ammonia salts.

Preferred compounds from the group of flavins are flavin adenine dinucleotide (FAD) and flavin mononucleotide (FMN).

Folic acid or its salts and/or flavins are advantageously contained in the inventive preparations, preferably each in quantities of 0.0001 to 5 wt.%, especially 0.01 to 1.5 wt.%, in each case relative to the total weight of the preparation.

The inventive cosmetic or dermatological topical preparations can be based on conventional formulation basics per se and can treat the skin in the sense of a dermatological treatment or a treatment in the sense of skin-care cosmetics.

Particularly advantageous preparations are furthermore obtained when the inventive active substances are combined with antioxidants.

It was not foreseeable that the active substances and combinations with an active content of arginine, ornithine, or citrulline and the aforesaid co-factors or the aforesaid combination with antioxidants would alleviate neurosensory hypersensitivity and itching. Furthermore, it was not foreseeable that they would lead to products that are tolerated by skin or that increase tolerance and in healthy skin does not interfere with autologous microflora in the skin.

Thus the objects cited in the foregoing are attained.

Typical troublesome neurosensory phenomena that are associated with the terms "stinging" and "sensitive skin" are skin reddening, pins and needles, pricking, tension, burning of the skin, and itching. They can be evoked by stimulating environmental conditions, e.g. massage, the effect of surfactants, weather factors such as the sun, cold, and dryness, but also damp heat, heat radiation, and UV radiation, e.g. from the sun.

Surprisingly, in accordance with the invention the symptoms of sensitive skin and itching are alleviated or prevented in diseases of the skin such as e.g. atopy.

The inventive antioxidants can advantageously be selected from the group of usual cosmetic and dermatological antioxidants, especially from the group comprising tocopherols and their derivatives, especially α-tocopherol or α-tocopheryl esters, in particular α-tocopheryl acetate, furthermore sesamol, bile acid derivatives such as methyl, ethyl, propyl, amyl, butyl, and lauric gallate, the coniferylbenzoate of benzoin resin, nordihydroguaiacinic acid, nordihydroguaiaretic acid,

butylhydroxyanisol, butylhydroxytoluene, ascorbic acid, citric acid, phosphoric acid, lecithin, trihydroxybutyrophenon, carotenes, vitamin A and its derivatives, especially retinylpalmitate, ascorbic acid, ascorbylpalmitate, dilaurylthiodipropionate, distearylthiodipropionate, monoisopropylcitrate, thiodipropionic acid, EDTA and EDTA derivatives, cysteine, glutathione and esters, uric acid, lipoic acid and esters, carotenes, heavy metal complex formers such as delta-amino lavulinic acid, and phytin acid.

The inventive cosmetic or dermatological preparations contain preferably 0.01 to 10 wt.%, but especially 0.1 to 6 wt.%, relative to the total weight of the preparations, of one or a plurality of the substances from the group of antioxidants.

It is preferred to select the inventive antioxidants from the group of tocopherols and their derivatives.

Moreover, the preparations advantageously also contain urea. The urea content is for instance 0.01 – 30 wt.%, especially 0.1 – 10 wt.%, relative to the total weight of the preparations.

For application, a sufficient quantity of the preparation is applied to the skin in the manner normal for cosmetic and dermatological products.

Especially preferred are skin care and hand care preparations, sun screen and after-sun preparations, and bath and shower preparations having a skin-care function.

Dermatological and cosmetic preparations in accordance with the invention can come in different forms. Thus e.g. aqueous, alcoholic, or aqueous-alcoholic solutions, oil-in-water (O/W) emulsions, water-in-oil (W/O) emulsions, multiple emulsions (e.g. water-in-oil-in-water (W/O/W) emulsions), gels, hydrodispersions, solid blocks and aerosols can contain the aforesaid combinations of active substances.

The inventive topical preparations can contain the usual adjuvants such as emulsifiers and preservatives.

Those cosmetic and dermatological preparations that are in the form of sun screens are also preferred. These advantageously also contain at least one UVA filter and/or at least one UVB filter and/or at least one in organic pigment.

However, those preparations that are applied after the skin has been exposed to light, that is, after-sun products, are also extremely advantageous. With such preparations, whether additional UV filter substances should be used or not is left to the discretion of the one skilled in the art.

Cosmetic preparations in accordance with the invention for protecting the skin from UV rays can be in different forms, such as they are e.g. normally used for this type of preparation. Thus they can be e.g. an aqueous, alcoholic, or aqueous alcoholic solution, a water-in-oil (W/O) emulsion or an oil-in-water (O/W) emulsion or a multiple emulsions, for instance water-in-oil-in-water (W/O/W) emulsion,

a gel, a hydrodispersion, a solid block, or an aerosol.

The inventive topical preparations can contain cosmetic adjuvants such as are normally used in such preparations, e.g. preservatives, bactericides, fragrances, anti-foaming agents, dyes, pigments that have a dying action, thickening agents, surfactant substances, emulsifiers, softening substances, wetting and/or moisture-retaining substances, fats, oils, waxes, or other conventional constituents of a cosmetic formulation such as alcohols, polyols, polymers, foam stabilizers, electrolytes, organic solvents, and silicone derivatives.

If the cosmetic or dermatological preparation is a solution or lotion, the following can be used for solvents:

- water or aqueous solutions;
- oils, such as triglycerides of capric acid or caprylic acid, but preferably also castor oil;

- Fats, waxes, and other natural and synthetic fatty bodies, preferably esters of fatty acids with alcohols having a low C number, e.g. with isopropanol, propylene glycol, or glycerol, or esters of fatty alcohols with alkane acids having a low C number or with fatty acids;

- Alcohols, diols, or polyols having a low C number, and their ethers, preferably ethanol, isopropanol, propylene glycol, glycerol, ethylene glycol, ethylene glycolmonoethyl or monobutyl ether, propylene glycol monomethyl,

- Monoethyl or monobutyl ether, diethylene glycol monomethyl or monoethyl ether and similar products.

In particular mixtures of the aforesaid solvents are used. Water can be another constituent in alcoholic solvents.

Emulsions in accordance with the invention, e.g. in the form of a sun-screen cream, sun-screen lotion, or suntan lotion are advantageous and contain e.g. the aforesaid fats, oils, waxes, and other fatty bodies, as well as water and an emulsifier as it is normally used for such a formulation.

Cosmetic and dermatological preparations for treating and caring for the skin can be gels that, in addition to the active substances and solvents normally used for them, also contain organic thickening agents, e.g. gum arabic, xanthan gum, sodium alginate, cellulose derivatives, preferably methyl cellulose, hydroxymethyl cellulose, hydroxyethyl cellulose, hydroxypropyl cellulose, hydroxypropylmethyl cellulose, and inorganic thickening agents, e.g. aluminum silicates such as for instance bentonites, or a mixture of polytheylene glycol and polyethylene glycol stearate or distearate. The thickening agent is contained in the gel e.g. in a quantity between 0.1 and 30 wt.%, preferably between 0.5 and 15 wt.%.

Inventive gels normally contain alcohols having a low C number, e.g. ethanol, isopropanol, 1.2-propandiol, glycerol, and water or one of the aforesaid oils in the presence of a thickening agent, that

in oily-alcoholic gels is preferably silicon dioxide or an aluminum silicate, and in aqueous-alcoholic or alcoholic gels is preferably a polyacrylate.

Hydrodispersons are dispersions of a liquid, semi-solid, or solid internal (discontinuous) lipid phase in an external aqueous (continuous) phase.

In contrast to O/W emulsions, which are distinguished by a similar phase arrangement, hydrodispersions are largely free of emulsifiers. Like emulsions, hydrodispersions are metastable systems and tend to convert to a condition of two discrete cohesive phases. In emulsions, the selection of a suitable emulsifier inhibits phase separation.

In hydrodispersions of a liquid lipid phase in an exterior aqueous phase, the stability of such a system can be assured for instance in that a gel structure in which the lipid droplets are suspended stably is constructed in the aqueous phase.

Solid bars in accordance with the invention can contain e.g. natural or synthetic waxes, fatty alcohols, or fatty acid esters. Lipstick-style bars are preferred.

Suitable as propellants for inventive cosmetic or dermatological preparations that can be sprayed from aerosol containers are the normal, known, highly volatile, liquefied propellants, for instance hydrocarbons (propane, butane, isobutane), which can be used

alone or in mixtures. Using compressed air is also advantageous.

Naturally one skilled in the art also knows that per se there are non-toxic propellant gases that fundamentally would be suitable for the present invention, but that should not be used because they may be hazardous to the environment or because of some other factor, especially fluorocarbons and hydrochlorofluorocarbons.

Preferably the inventive preparations can also contain substances that absorb UV radiation in the UVB range, the total quantity of the filter substances being e.g. 0.1 wt.% to 30 wt.%, preferably 0.5 to 10 wt.%, especially 1 to 6 wt.%, relative to the total weight of the preparation, in order to provide cosmetic preparations that protect the skin from the entire range of ultraviolet radiation. They can also act as sunscreens.

The UVB filters can be oil-soluble or water-soluble. Oil-soluble substances that can be used include e.g.:

- 3-benzylidene camphor derivatives, preferably 3-(4-methylbenzyliden) camphor, 3-benzylidene camphor;
- 4-aminobenzoic acid derivatives, preferably 4-(dimethylamino)-benzoic acid (2-3thylhexyl) ester, 4-(dimethylamino)benzoic acid amyl ester;
- Esters of cinnamic acid, preferably 4-methoxycinnamic acid (2-ethylhexyl) ester, 4-methoxycinnamic acid isopentyl ester;
- Esters of salicylic acid, preferably

salicylic acid (2-ethylhexyl) ester, salicylic acid (4-isopropylbenzyl) ester, salicylic acid homomenthyl ester;

- Derivatives of benzophenone, preferably 2-hydroxy-4-methoxybenzophenone, 2-hydroxy-4-methoxy-4'-methylbenzophenone, 2,2'-dihydroxy-4-methoxybenzophenone;
- Esters of benzal malonic acid, preferably 4-methoxybenzal malonic acid die(2-ethylhexyl)ester;
- 2,4,6-trianilino-(p-carbo-2'-ethyl-1'-hexyloxy)-1,3,5-triazine.

Water-soluble substances that can be used include e.g.:

- Salts of 2-phenylbenzimidazole-5-sulfonic acid like its sodium, potassium, or triethanol ammonium salt, and sulfonic acid itself;
- Sulfonic acid derivatives of benzophenones, preferably 2-hydroxy-4-methoxybenzophenone-5-sulfonic acid and its salts;
- Sulfonic acid derivatives of 3-benzylidene camphor, such as e.g. 4-(2-oxo-3-bornylidene methyl) benzene sulfonic acid, 2-methyl-5-(2-oxo-3-bornylidene methyl) sulfonic acid and its salts.

The subject-matter of the invention is also the combination of inventive active substances with one or a plurality of UVB filters and inventive cosmetic or dermatological preparations that also contain one or a plurality of UVB filters.

It can also be advantageous to combine the active substances with UVA filters that were previously normally contained in cosmetic and/or dermatological. These substances are preferably derivatives of dibenzoylmethane, in particular 1-(4'-tert. butylphenyl)-3-(4'-methoxyphenyl)propane-1,3-dion and 1-phenyl-3-(4'-isopropylphenyl)propane-1,3-dion. These combinations and preparations that contain these combinations are also the subject-matter of the invention. The quantities used for the UVB combination can be employed.

Advantageous preparations are obtained when the inventive active substances are combined with UVA and UVB filters.

Combinations of the inventive active substances with one or a plurality of antioxidants and one or a plurality of UVA filters and/or one or a plurality of UVB filters are also particularly advantageous in accordance with the invention.

The cosmetic or dermatological preparations can also contain inorganic pigments that are normally used in cosmetics for protecting the skin from UV radiation. These are oxides of titanium, zinc, iron, zirconium, silicon, manganese, aluminum, cerium, and mixtures thereof, as well as variants in which the oxides are the active agents. Titanium dioxide-based pigments are particularly preferred.

Subject-matter of the invention is also the method for producing the inventive topical preparation, which method is characterized in that the active substances are worked into cosmetic or dermatological formulations

in a manner known per se.

Provided there is no information to the contrary, all data regarding quantities, proportions, and percentages relate to the weight and total quantity or to the total weight of the preparations.

The following examples are intended to clarify the present invention without restricting the invention.

Example 1

Sun gel LF 4 (transparent)

	Wt.%
L-arginine hydrochloride	10
Benzophenone-4	0.5
Phenylbenzimidazole sulfonic acid	1.3
Acrylamide/sodium acrylate copolymer	1.6
Ethanol	5.0
Glycerol	15.0
NaOH (15%)	as necessary
Fragrance, preservatives	as necessary
Water, demin. (fully desalinated)	to 100.0

Example 2

Hydrodispersion

	Wt.%
L-ornithine hydrochloride	5.0
Phenyl trimethicone	1.0
Carbomer (Carbopol 981)	1.0
Hydroxypropylmethyl cellulose	2.0
Butylene glycol	3.0
Tromethamine	as necessary

EDTA solution (14%)	0.5
Ethanol	5.0
Fragrance, preservatives	as needed
Water, demin. (fully desalinated)	to 100.0

Example 3

Suntan lotion O/W

	Wt.%
L-arginine hydrochloride	5.0
Octylmethoxycinnamate	5.0
Butyl methoxydibenzoylmethane	1.0
Cetearyl alcohol + PEG-40 castor oil + sodium cetearyl sulfate	2.5
Glyceryl lanolate	1.0
Lauryl methicone copolyol	0.5
Mineral oil (DAB 9)	5.0
Caprylic/capric triglycerides	5.0
Acrylamide/sodium acrylate copolymer	0.3
Cyclomethicon	2.0
TiO_2	1.0
Glycerol	3.0
EDTA solution (14%)	0.5
Ethanol	5.0
Fragrance, preservatives	as necessary
Water, demin. (fully desalinated)	to 100.0

Example 4

Skin lotion W/O

	Wt.%
L-arginine hydrochloride	2.5
Folic acid	0.1
Cyclomethicon	3.0
PEG-1-glycerol sorbitan oleostearate	1.7

PEG-7 hydrated castor oil	6.3
Mineral oil (DAB 9)	13.0
Caprylic/capric triglycerides	13.0
Glycerol	4.0
$MgSO_4$	0.7
Fragrance, preservatives	as necessary
Water, demin.	to 100.0

Example 5

Daily skin crème O/W

	Wt.%
L-arginine hydrochloride	5.0
L-ornithine	1.0
PEG-5 glyceryl stearate	2.00
Glyceryl stearate	3.00
Cyclomethicon	3.00
Caprylic/capric triglycerides	3.00
Cetyl alcohol	3.00
Octyl methoxycinnamate	2.50
Ethanol	1.00
Hyaluronic acid	0.05
Tocopheryl acetate	0.50
Glycerol	4.00
Fragrance, preservatives	as necessary
Water, demin.	to 100.0

Example 6

W/O crème

	Wt.%
L-citrulline	2.5
L-arginine hydrochloride	2.5
FAD	0.1
FMN	0.05

PEG-22-dodecyl glycol copolymer	3.0
Cetyl dimethicone copolyol	2.0
Cyclomethicon	4.0
Mineral oil (DAB 9)	4.0
Caprylic/capric triglycerides	4.0
Glycerol	4.00
Fragrance, preservatives	as necessary
Water, demin.	to 100.0

Example 7

W/O crème

	Wt.%
L-ornithine hydrochloride	2.5
L-citrulline	2.5
L-arginine hydrochloride	2.5
FAD	0.1
FMN	0.05
PEG-22-dodecyl glycol copolymer	3.0
Cetyl dimethicone copolyol	2.0
Cyclomethicon	4.0
Mineral oil (DAB 9)	4.0
Caprylic/capric triglycerides	4.0
Glycerol	4.00
Fragrance, preservatives	as necessary
Water, demin.	to 100.0

Example 8

After-sun lotion

	Wt.%
L-arginine hydrochloride	5.0
Folic acid	0.1
Urea	2.5

Cetearyl alcohol + PEG-40 castor oil + sodium cetearyl sulfate	2.50
Glyceryl stearate SE	0.60
Mineral oil (DAB 9)	4.00
Caprylic/capric triglycerides	2.00
Shea butter	2.00
Avocado oil	2.00
Tocopheryl acetate	3.00
Acrylamide/sodium acrylate copolymer	0.30
Glycerol	4.00
Hyaluronic acid	0.05
Bisabolol	0.05
Fragrance, preservatives	as necessary
Water, demin.	to 100.0

Example 9

Shower lotion

	Wt.%
L-arginine hydrochloride	10.0
Folic acid	1.0
Sodium laureth sulfate	12
Cocamidopropyl betaine	5
Cocamide DEA	1
PEG-8	1
Soybean oil	1
Citric acid	0.1
Sodium chloride	0.2
Fragrance	0.1
Water, demin.	to 100.0

Example 10

W/O crème

	Wt.%
L-ornithine hydrochloride	2.5
L-citrulline	2.5
L-arginine hydrochloride	2.5
FAD	0.1
FMN	0.05
Folic acid	0.1
Tocopheryl acetate	1.0
Urea	2.5
PEG-22-dodecyl glycol copolymer	3.0
Cetyl dimethicone copolyol	2.0
Cyclomethicon	4.0
Mineral oil (DAB 9)	4.0
Caprylic/capric triglycerides	4.0
Glycerol	4.00
Fragrance, preservatives	as necessary
Water, demin.	to 100.0

Test report

The excellent effect of the inventive active substances is demonstrated with the following test report. The lotion from Example 4, but with an active substance content of 5 wt.% L-arginine and without folic acid and fragrance, is used in a "stinging test" with 5 wt.% lactic acid in water as "stinger", as in Frosch and Kligman (Peter J. Frosch and Albert M. Kligman: "A method for appraising the stinging capacity of topically applied substances", J. Soc. Cosmet. Chem. 28, 197209, 1977).

After one week's contra-lateral product application (two times daily), the stinging potential of 5% lactic acid is determined after a single application to the cheeks. First on the one cheek and approx. 1 hour later, after the irritation has cleared, on the other cheek. The stinging potential of 5% lactic acid is significantly reduced on the cheeks previously treated with 5% L-arginine.

Patent claims

1. Use of one or a plurality of compounds selected from the group of L-arginine, L-ornithine, and L-citrulline or their salts, acid addition salts, esters, or amides, where necessary with the addition of folic acid or its salts and/or one or a plurality of compounds selected from the group of flavins, for prophylactic purposes and/or treatment of neurosensory phenomena.

2. Use of cosmetic and dermatological topical preparations having a content of one or a plurality of compounds selected from the group of L-arginine, L-ornithine, and L-citrulline or their salts, acid addition salts, esters, or amides, where necessary with the addition of folic acid or its salts and/or one or a plurality of compounds selected from the group of flavins, for prophylactic purposes and/or treatment of neurosensory phenomena.

3. Use in accordance with claim 2, characterized in that the preparations contain L-arginine.

4. Use in accordance with claim 2, characterized in that the preparations contain folic acid and/or one or a plurality of compounds selected from the group of flavins.

5. Use in accordance with claim 2, characterized in that the preparations contain at least one antioxidant.

6. Use in accordance with claim 2, characterized in that the preparations contain urea.

7. Use in accordance with claim 2, characterized in that the preparations contain at least one UVA filter and/or at least one UVB filter and/or at least one inorganic pigment.

8. Use in accordance with claim 2, characterized in that the preparations contain L-arginine, folic acid, one or a plurality of compounds selected from the group of flavins, at least one antioxidant, urea, and where necessary at least one UVA filter and/or at least one UVB filter and/or at least on inorganic pigment.